European Journal of Medicinal Chemistry 302 (2026) 118384

Contents lists available at ScienceDirect

European Journal of Medicinal Chemistry

journal homepage: www.elsevier.com/locate/ejmech

Research paper

Triazole-containing xanthone-furanose/pyranose hybrids: synthesis of potential α-glucosidase inhibitors

Carlos D. García-Mejía [a], Julio César Almanza-Pérez [b], Luis Fernando Cofas-Vargas [c], Abigail Aragón-Morales [b], Antonio Nieto-Camacho [a], Enrique García-Hernández [a], Eduardo Hernández-Vázquez [a,*]

[a] Instituto de Química, Universidad Nacional Autónoma de México, Circuito Exterior, Ciudad Universitaria, Coyoacán, 04510, CDMX, México
[b] Departamento de Ciencias de la Salud, Universidad Autónoma Metropolitana, Unidad Iztapalapa, CDMX, México
[c] Institute of Fundamental Technological Research, Polish Academy of Sciences, Pawińskiego 5B, 02-106, Warsaw, Poland

ARTICLE INFO

Keywords:
T2DM
Xanthone
Triazole
Carbohydrates
α-glucosidase inhibitors

ABSTRACT

A collection of xanthone-carbohydrate hybrids is reported as potential α-glucosidase inhibitors. The inhibitory activity of the xanthone core and the poly-hydroxylated commercially available drugs inspired the design of the compounds. Accordingly, both moieties were linked through a triazole core prepared by a copper-catalyzed alkyne-azide cycloaddition. After *in vitro* testing, compound **17f** was identified as the most remarkable compound, with an IC_{50} of 14.9 ± 1.7 μM (acarbose had an IC_{50} of 7.3 ± 0.3 mM). Additionally, molecular docking studies suggested that the hybrids bind to the allosteric site, which explains the non-competitive or mixed inhibition found in enzymatic kinetics; the stability of the complex was confirmed through molecular dynamics simulation. Furthermore, an oral sucrose tolerance test (OSTT) in both healthy and diabetic mice demonstrated that benzoxanthone derivatives **17f** and **18f** prevent the hyperglycemic peak that occurs after sucrose administration. Although α-glucosidase inhibition is a key mechanism of action for xanthone **17f**, it also improved plasma glucose levels after 60 min of sucrose administration in diabetic mice, resulting in a decrease of 42 % compared to initial glucose levels and showing better reduction than acarbose (reduction of 22 %), suggesting a complementary antidiabetic effect.

1. Introduction

Among chronic diseases, type 2 diabetes mellitus (T2DM) persists as one of the most threatening issues of the 21st century. High glucose levels in blood plasma and abnormal metabolism of lipids and proteins characterize T2DM [1], leading to serious complications and several organ failures. Additionally, the rising morbidity and mortality rates of T2DM position it as one of the principal causes of death worldwide [2].

In 2021, the International Diabetes Federation reported that 537 million adults were living with T2DM, and this number could increase to 643 million by 2030 [3]. Therefore, improving the current therapeutic arsenal to treat this metabolic disease becomes a priority in Medicinal Chemistry [4]. In this sense, α-glucosidase inhibitors offer a complementary strategy to control postprandial plasma glucose levels by decreasing intestinal absorption [5,6]. The improvement of glycemic levels occurs without producing hypoglycemia or weight gain [7]. Besides, treatment with α-glucosidase inhibitors is associated with lowering the risk of cardiovascular disease, one of the most frequent vascular complications in diabetic patients [8].

Traditionally, treatment with α-glucosidase inhibitors includes acarbose (**1**), miglitol (**2**), and voglibose (**3**) (Fig. 1A); however, these carbohydrate-related drugs are associated with undesired gastrointestinal side effects and the potential for liver damage [9]. Therefore, searching for new compounds with demonstrated inhibitory activity against this enzyme becomes an attractive approach for developing innovative antidiabetic drugs [10,11].

In recent years, the 9*H*-xanth-9-one core has received massive attention due to its diverse range of biological applications [12,13]. Specifically, several studies confirm that xanthone-containing compounds can inhibit α-glucosidase [14–16]. Previous reports have shown that activity increases when an ester group acts as a linker between the xanthone core and aromatic moieties. Unfortunately, esters may suffer

* Corresponding author.
E-mail address: ehervaz@iquimica.unam.mx (E. Hernández-Vázquez).

https://doi.org/10.1016/j.ejmech.2025.118384
Received 1 October 2025; Received in revised form 10 November 2025; Accepted 16 November 2025
Available online 24 November 2025

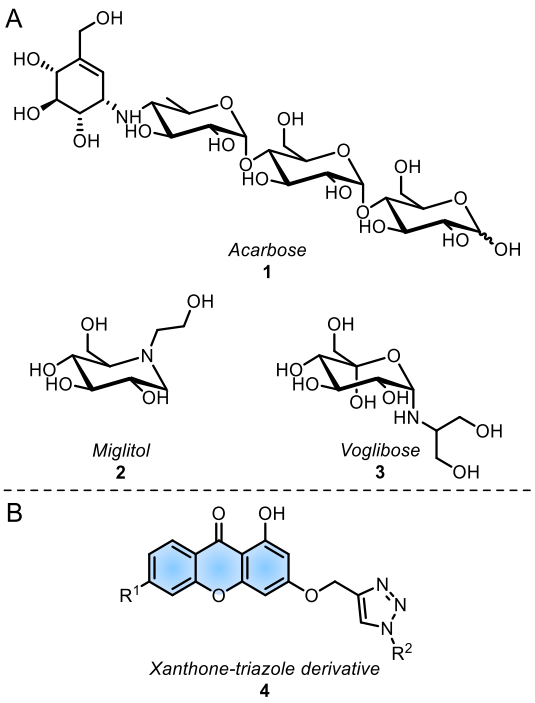

Fig. 1. A) Commercially available α-glucosidase inhibitors; B) xanthone derivatives act as non-competitive α-glucosidase inhibitors.

metabolic degradation, thus limiting their future applications [17]. As an effort to overcome this issue, Ye and co-workers replaced the ester group with a 1,2,3-1*H*-triazole ring, resulting in a significant α-glucosidase inhibition, especially when the xanthone is substituted at C6 (**4**, Fig. 1B) [16].

Considering the above, we envisioned that hybridization of both pharmacophores –the xanthone heterocycle and carbohydrates– could enhance the inhibition of α-glucosidase (Fig. 2). Due to its metabolic stability, 1,2,3-1*H*-triazole acted as the linker and was constructed by a Copper(I)-catalyzed Azide-Alkyne Cycloaddition (CuAAC). Regarding the sugar moiety, we selected glucose (in both furanose and pyranose cyclic structures), as shown in commercially available inhibitors. In addition, we employed xanthones bearing electron-donating, electron-withdrawing, and steric substituents at the C6 position.

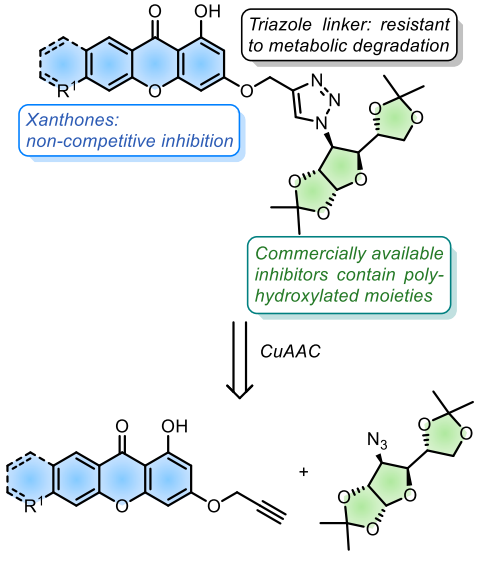

Fig. 2. Design and retrosynthesis of xanthone-furanose/pyranose hybrids.

The designed compounds were *in vitro* tested against *Saccharomyces cerevisiae* α-glucosidase. At the same time, enzymatic kinetics and molecular docking helped us to analyze the characteristics of the enzyme inhibition. Finally, an oral sucrose tolerance test demonstrated the potential antidiabetic effect of xanthone-furanose/pyranose hybrids.

2. Results and discussion

2.1. Chemistry

The synthesis of xanthones-furanose/pyranose derivatives implied the construction of a triazole linker through a *click* chemistry approach (Fig. 2). Under this premise, the synthetic adventure commenced with the preparation of azide-containing carbohydrates, employing a previously reported divergent route [18,19]. First, we transformed D-glucose (**5**) into the acetonide **6** –using acetone and catalytic sulfuric acid–. Subsequently, epimerization of the protected glucose through a two-step sequence (oxidation with NaOCl followed by a diastereoselective reduction with sodium borohydride) resulted in the isolation of **8** (*R* isomer) in good yield (85 %). Finally, the conversion of the hydroxyl group to triflate and subsequent bimolecular substitution (S_N2) gave access to the azido-furanose **9** in 78 % yield (Scheme 1).

For the pyranose fragment, D-glucose (**5**) reacted with acetic anhydride in the presence of pyridine to provide the peracetylated compound **10** (93 %). Afterward, a nucleophilic attack with azide at the anomeric carbon afforded pyranose **11** in 95 % yield (Scheme 1).

On the other hand, we synthesized the *9H*-xanthen-9-one nuclei by condensing the corresponding salicylic acid (**12**) and phloroglucinol (**13**) in the presence of Eaton's reagent [20]. These conditions afforded the xanthones **14** in moderate to good yields (20–74 %). Although previously reported methods used xanthones without purification [20,21], we corroborated the importance of removing phosphorus byproducts to avoid interference in subsequent steps. Thereafter, we focused on obtaining alkynes **16** through an S_N2 reaction between the corresponding xanthones and propargyl bromide (**15**). The reaction afforded the 3-propargyloxyxanthones in yields ranging from 51 to 84 % (Scheme 2); nevertheless, the transformation was hampered by the low solubility of both compounds and high affinity for silica gel.

It is worth noting that despite the xanthones **13a-i** possess two potential nucleophilic centers, TLC and ^{1}H NMR spectra indicated that the reaction provided only the desired C3-alkylated isomer. The regioselectivity of the transformation can be attributed to the low nucleophilicity of the hydroxyl group at C1, as it forms a hydrogen bond with the carbonyl group of the xanthone, which is evidenced by a chemical shift of 12.3–13.0 ppm in the ^{1}H NMR spectra (Fig. 3) and is conserved in all propargylated xanthones. Instead, the hydroxyl group at C3 of the C1-alkylated isomer should present a typical chemical shift of 9.00–9.40 ppm [22].

Once we obtained both starting materials necessary for the CuAAC protocol, we proceeded to construct the triaza-heterocycle using copper (II) sulfate pentahydrate as a source of Cu(I) and sodium L-ascorbate as an additive (Scheme 2) [23]. With this methodology, we prepared a collection of triazoles in moderate yields (17–52 %, Table 1) whose sugar moiety consisted of a furanose ring. Additionally, we became interested in investigating the influence of the pyranose core (specifically, D-glucose) on enzymatic inhibition, so we synthesized a second group of triazoles (**18a-f**), which were obtained in similar yields (13–81 %, Table 1).

2.2. Preliminary α-glucosidase inhibition screening

Once both series of xanthone-carbohydrate hybrids were synthesized and characterized, we tested their potential for inhibiting *Saccharomyces cerevisiae* α-glucosidase at a concentration of 100 μM [11]. The compounds showed an encouraging reduction of activity ranging from 59 to

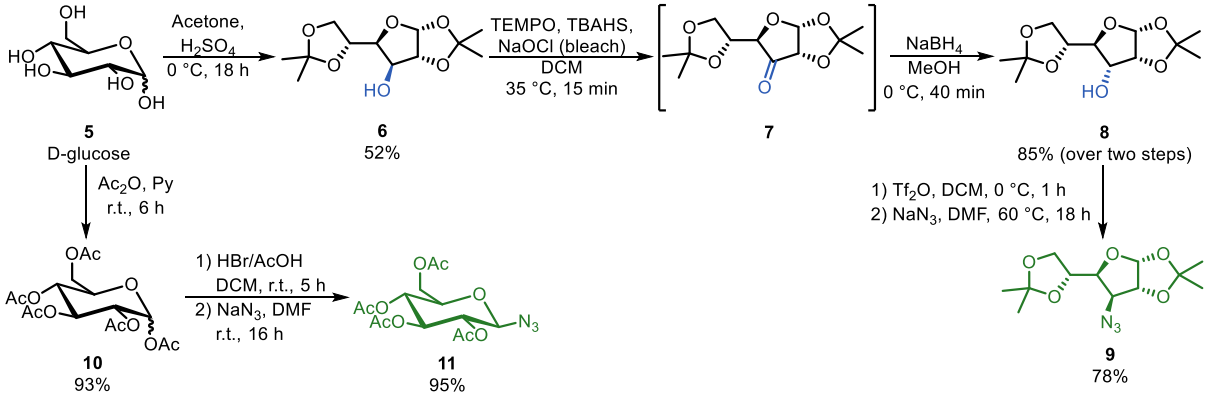

Scheme 1. Synthesis of the azide-containing carbohydrates.

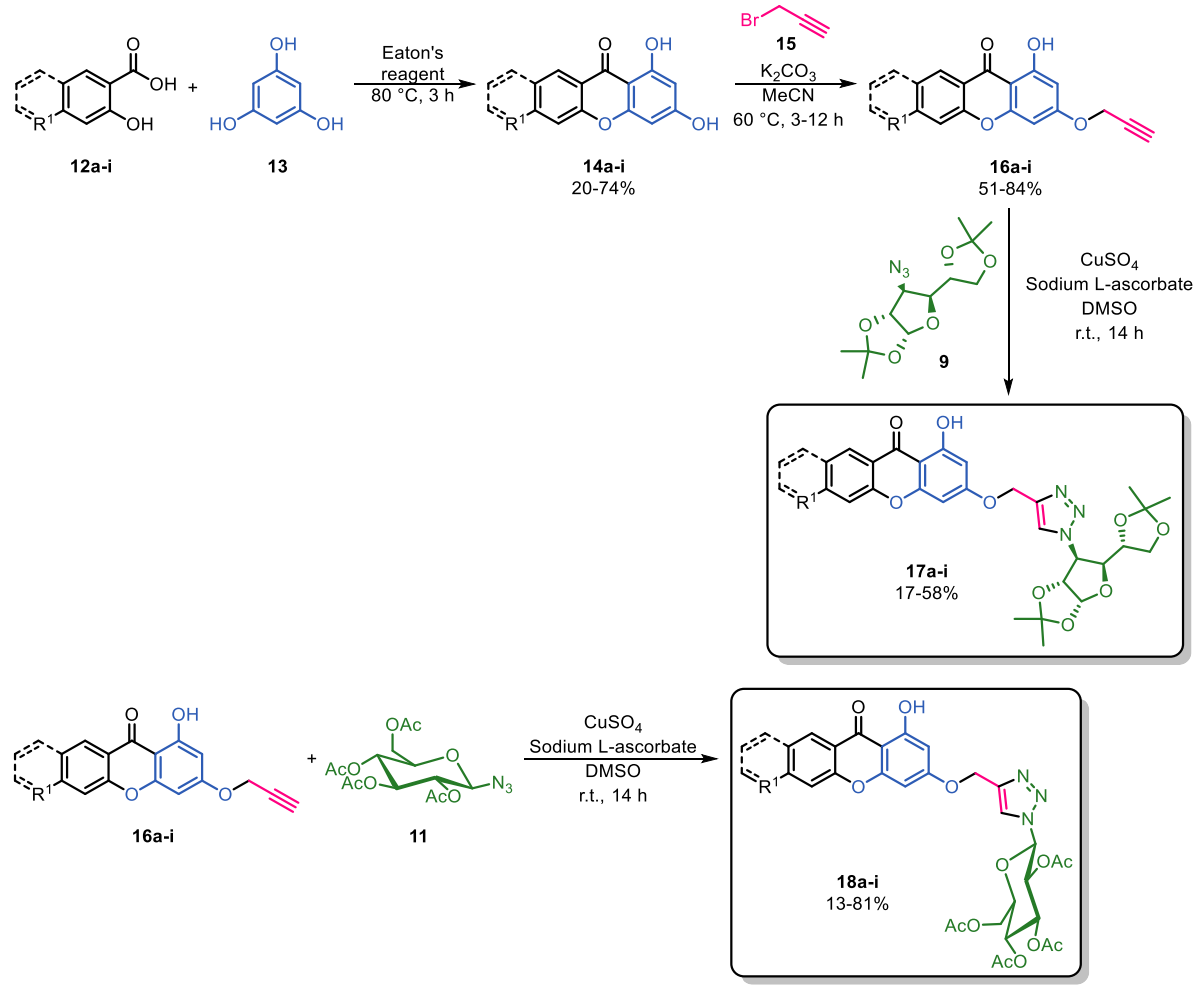

Scheme 2. Synthetic steps for the obtention of xanthone-furanose/pyranose hybrids.

97 %; to our delight, the methoxylated compound **18c** and benzoxanthones **17f** and **18f** were the most active compounds, reaching inhibition percentages above 90 % (Fig. 4). We also tested quercetin (56 % inhibition at 16 μM) and the commercial drug acarbose (59 % inhibition at 10 mM); curiously, the oligosaccharide acarbose had a minimal inhibition of α-glucosidase, as previously reported [24].

According to previously published works [16], along with the *in vitro* screening, a methoxy group in the xanthone increased the α-glucosidase inhibition (**18c**, 97.5 ± 0.2 %; Fig. 4). Thus, we shifted this oxygenated group to other positions of the xanthone core to analyze its influence on biological activity. Following this idea, we oxidized *o*-vanillin (**19**) to the corresponding salicylic acid employing the Tollens reagent [25]. The constructed 3-methoxysalicylic acid (**12g**) afforded the compounds **17g** and **18g** in comparable yields (58 and 63 %, respectively; Table 2). Similarly, we prepared triazoles **17h** and **18h** from the commercially available 7-methoxysalicylic acid (**12h**).

Since compounds **17f** and **18f** (linear benzoxanthones) exhibited a promising α-glucosidase inhibition (94.4 ± 0.9 and 92.4 ± 1.3 %,

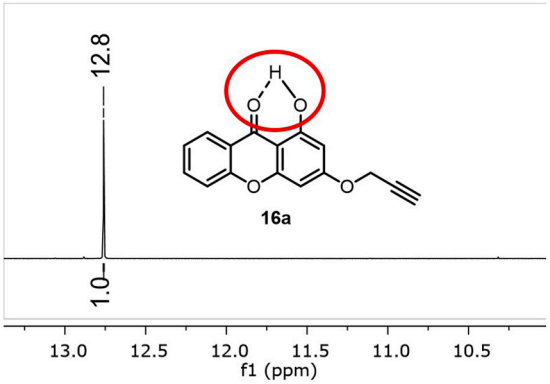

Fig. 3. The high chemical shift of the hydroxy group at C1 is a consequence of the hydrogen bond. The conservation of this signal confirmed the regioselectivity of the reaction.

respectively), we envisioned the synthesis of angular benzoxanthones. The preparation of both examples followed a similar approach to previous xanthone-carbohydrate hybrids (Scheme 2).

Having in hand the second generation of triazole derivatives (Table 2), we evaluated their activity against hydrolase. Unfortunately, the percentage of α-glucosidase inhibition decayed when the methoxy group is located at C5 and C7 (Fig. 4), confirming the reported findings by Ye and coworkers [16]. Likewise, angular benzoxanthones (**17i**, 81.3 ± 0.3 %; and **18i**, 78.3 ± 3.5 %) showed less inhibitory activity than their linear analogs (**17f**, 94.4 ± 0.9 %; and **18f**, 92.4 ± 1.3 %).

The structure-activity relationship revealed some relevant features that enhance enzyme inhibition (Fig. 5). First, pyranose-containing xanthones exhibited a slightly higher activity than furanose derivatives, but this tendency was inverted in the case of benzoxanthone derivatives – xanthone **17f** (94.4 ± 0.9 %) > **18f** (92.4 ± 1.3 %); **17i** (81.3 ± 0.3 %) > **18i** (78.3 ± 3.5 %). Regarding substituents attached to the xanthone core, position C6 is preferred, while electron-withdrawing groups, as fluor (**17d** and **18d**) or dichloro (**17e** and **18e**), diminished the inhibitory effect. In contrast, xanthones with a methoxy group at C6 showed the most notable activity (**18c**, 97.5 ± 0.2 %). We propose that the exceptional activity of linear benzoxanthones could be attributed to the enhancement of π-π stacking induced by the extra aromatic ring.

According to the above, we determined the IC_{50} of the most active compounds. In the case of the methoxylated example (**18c**), we found an IC_{50} value of 22.7 ± 6.9 μM. Similarly, benzoxanthones had IC_{50} values of 14.9 ± 1.7 and 20.7 ± 3.1 μM for **17f** and **18f**, respectively (Table S2). Notably, **17f** displayed a lower IC_{50} value than the controls (quercetin, 15.6 ± 1.7 μM; acarbose, 7.3 ± 0.3 mM).

2.3. Enzyme kinetics and Lineweaver-Burk plots

Based on the previous section, we considered the three most active xanthones (**17f**, **18c**, and **18f**) and acarbose (**1**) for an enzyme kinetic study. We evaluated the activity using 1/2 × IC_{50}, IC_{50}, and 2 × IC_{50} concentrations for each compound. The outcomes are captured on Lineweaver-Burk plots (Fig. 6).

As reported, acarbose acted as a competitive inhibitor (Fig. 6D) [26,27]. In the case of the hybrids **17f**, **18c**, and **18f**, the slope increased at higher concentrations of the compounds. Curiously, we observed different types of inhibition for the tested compounds. In Fig. 6A and B, the curves intersected the x-axis at the same point, indicating that the K_M (Michaelis-Menten constant) of the substrate for α-glucosidase is constant, and the Vmax decreased at higher concentrations. Thus, we might propose that hybrids **17f** and **18c** act as non-competitive inhibitors. By contrast, curves of **18f** show a typical behavior of a mixed inhibitor (Fig. 6C).

2.4. Toxicity assays

Before exploring the *in vivo* bioactivity of the most notable compounds in mice, we performed a toxicity study in the crustacean *Artemia salina* [28,29]. Acute assay indicated that benzoxanthones **17f** and **18f** exhibited a null or very low toxicity against the arthropods at 1, 10, and 100 μM. In the case of **18c**, its toxicity is negligible at 10 μM (1.8 % of deaths), but it increased to 21.9 % at 100 μM (Table S3). In addition, we evaluated the cytotoxicity of benzoxanthones **17f** and **18f** in a non-cancerous cell line (COS-7), observing a moderate growth inhibition at 50 μM (**17f**, 42.1 %; **18f**, 58.2 %).

Although an acute toxicity assay in mice was not performed, the OSTT *in vivo* assay (*vide infra*) indicated the lack of death or any appreciable toxicity to the rodents.

2.5. Oral sucrose tolerance test (OSTT)

Inspired by the *in vitro* results, we became interested in further evaluating the most active xanthones. Hence, the oral sucrose tolerance test can determine if compounds inhibit α-glucosidase *in vivo* by analyzing the hyperglycemic peak after administering a sucrose dose. We only considered the most active and less toxic compounds (**17f** and **18f**) and the control (acarbose, **1**) at a dose of 50 mg/kg administered orally in a single dose.

First, we performed the oral sucrose tolerance test in normoglycemic mice, using a previously reported protocol with minor modifications [30]. After sucrose administration, we detected a maximum peak (74.0 ± 5.1 %) at 30 min in the control group (vehicle, saline solution). Glycemia returned to basal levels after 60–90 min, indicating a normal metabolic state. In comparison, the acarbose group showed a 15.4 ± 4.1 % glycemia variation at 30 min and reached normal levels at 1 h; glucose levels even decreased to −22.7 ± 6.0 % after 90 min of sucrose administration. Both tested hybrids (**17f** and **18f**) avoided the glycemia peak detected in the control group (34.1 ± 7.6 % and 37.7 ± 2.2 %, respectively). This behavior suggested that xanthone-carbohydrate hybrids inhibited α-glucosidase, thereby preventing sucrose hydrolysis and, consequently, avoiding the glucose peak (Fig. 7A). A similar pattern is evident in Fig. 7C and shows the variation of blood glucose levels throughout the experiment. Acarbose (**1**) and benzoxanthones **17f** and **18f** avoided the increment of plasma glucose at 30 min after sucrose administration. Subsequently, the glucose concentration decreased to normal levels.

Also, we induced experimental diabetes in a second group of mice by administering streptozotocin (STZ) [31] and nicotinamide. The control group of diabetic mice exhibited a glycemia peak after 30 min of sucrose administration (62.7 ± 9.8 %), which returned to basal levels more slowly than in healthy mice. Unexpectedly, the acarbose group followed a similar pattern to the control group, reaching a maximum peak at 30 min (66.8 ± 12.7 %). This phenomenon could be attributed to the insulin deficiency, which, in genetically diabetic mice [32], and STZ-induced diabetic rats [33,34], increases the activity of intestinal disaccharidases. Therefore, a major dose of acarbose is required to produce significant effects. At 60 min after acarbose administration, we observed that glycemia returned to basal levels and continued decreasing to −22.4 ± 4.3 % after 120 min (Fig. 7B).

To our surprise, both xanthones diminished the glycemia peak at 30 min in diabetic mice. In the case of xanthone **18f**, the maximum peak reached 33.3 ± 7.5 % and rapidly dropped to basal levels (Fig. 7B). On the other hand, xanthone **17f** was the most remarkable compound, exhibiting a 20.2 ± 7.8 % variation in blood glucose levels, which confirms that α-glucosidase inhibition is the mechanism of action of the hybrids **17f** and **18f**. In the diabetic group, **17f** administration showed a variation of −18.4 ± 5.6 % at 60 min and reached a minimum peak at 90 min (−41.8 ± 7.8 %). These outcomes indicate a more pronounced anti-hyperglycemic effect than acarbose (Fig. 7B) and suggest a potential second biological activity.

Table 1
Scope of the xanthone-furanose/pyranose hybrids. Yields correspond to the CuAAC process.

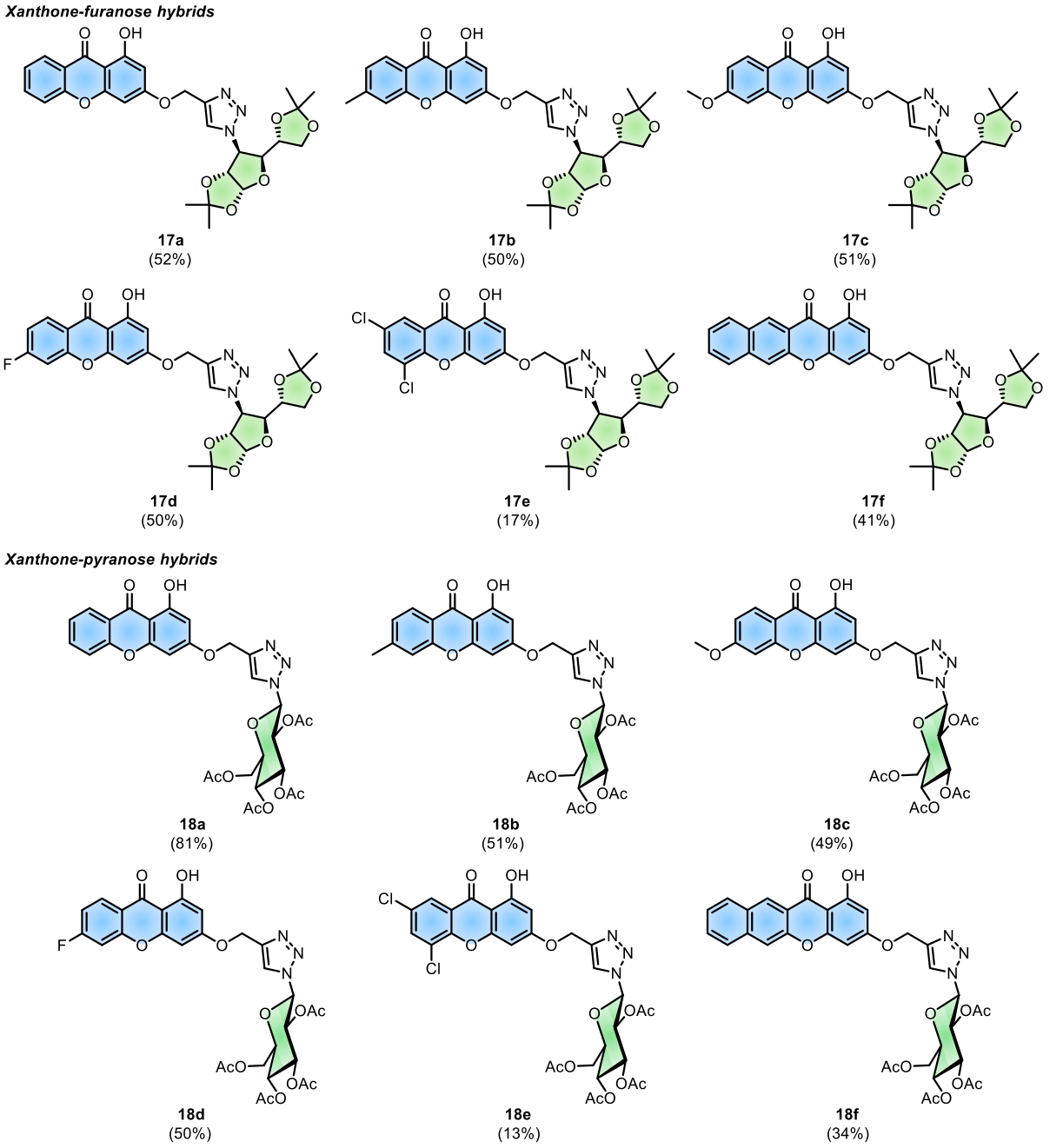

According to published works, natural xanthones can promote glucose uptake by activating the phosphoinositide 3-kinase (PI3K) [35] or the AMP-activated protein kinase (AMPK) signaling pathway [35,36]. Moreover, several reports indicate that natural or synthetic xanthones may prevent insulin resistance by scavenging ROS (thus diminishing oxidant stress) [37,38], inhibiting protein kinase C (PKC) [39,40], or protein tyrosine phosphatase 1B (PTP1B) [41,42]. Therefore, xanthone-carbohydrate hybrids could act through some of these pathways; however, more assays are required to elucidate the whole mechanism of action of these compounds.

Similar to normoglycemic, the three tested compounds prevented the peak of hyperglycemia in diabetic mice (Fig. 7D). Interestingly, only acarbose and benzoxanthone **17f** reduced glucose levels even lower than initial levels at 120 min, thus confirming the outcomes of Fig. 7B.

Finally, we analyzed the area under the curve (AUC). In normoglycemic mice, we observed a significant decrease in the acarbose area compared to the control group (Fig. 7E), while the areas of both hybrids decreased slightly. In contrast, **17f** significantly reduced the area for diabetic mice (Fig. 7F), surpassing the activity of acarbose. In future works, we will explore the pharmacological effects of deprotected xanthone-carbohydrate hybrids, as well as the replacement of sugar with other motifs.

2.6. Computational studies

Motivated by the *in vitro* outcomes, we became interested in

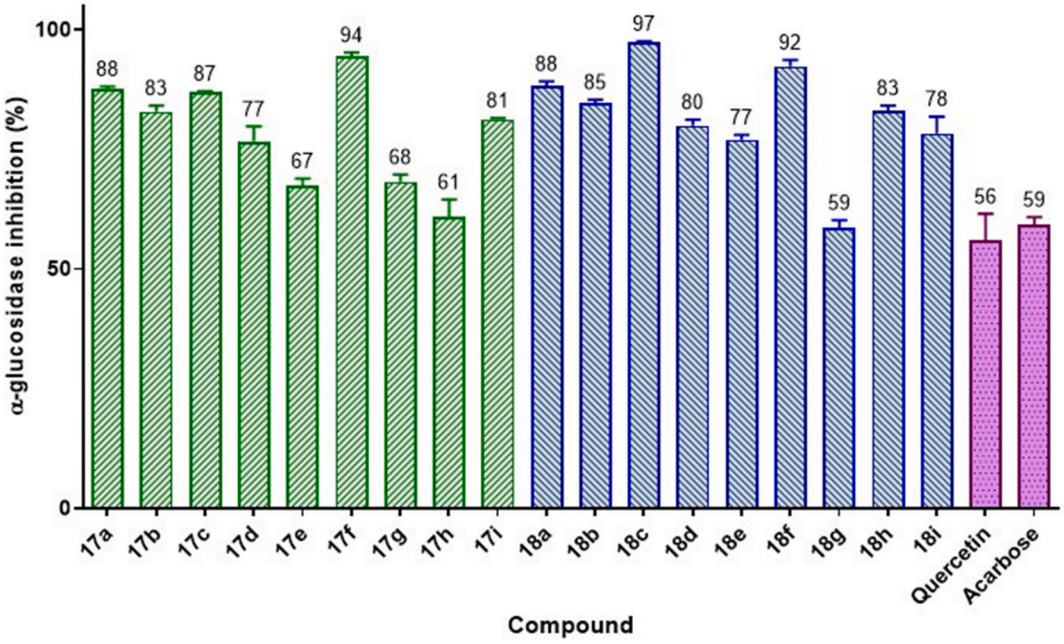

Fig. 4. Inhibition of *S. cerevisiae* α-glucosidase at 100 μM for the two series of xanthone-carbohydrate hybrids. Quercetin was tested at 16 μM, while Acarbose was tested at 10 mM (Table S1).

Table 2
Second generation of triazole derivatives.

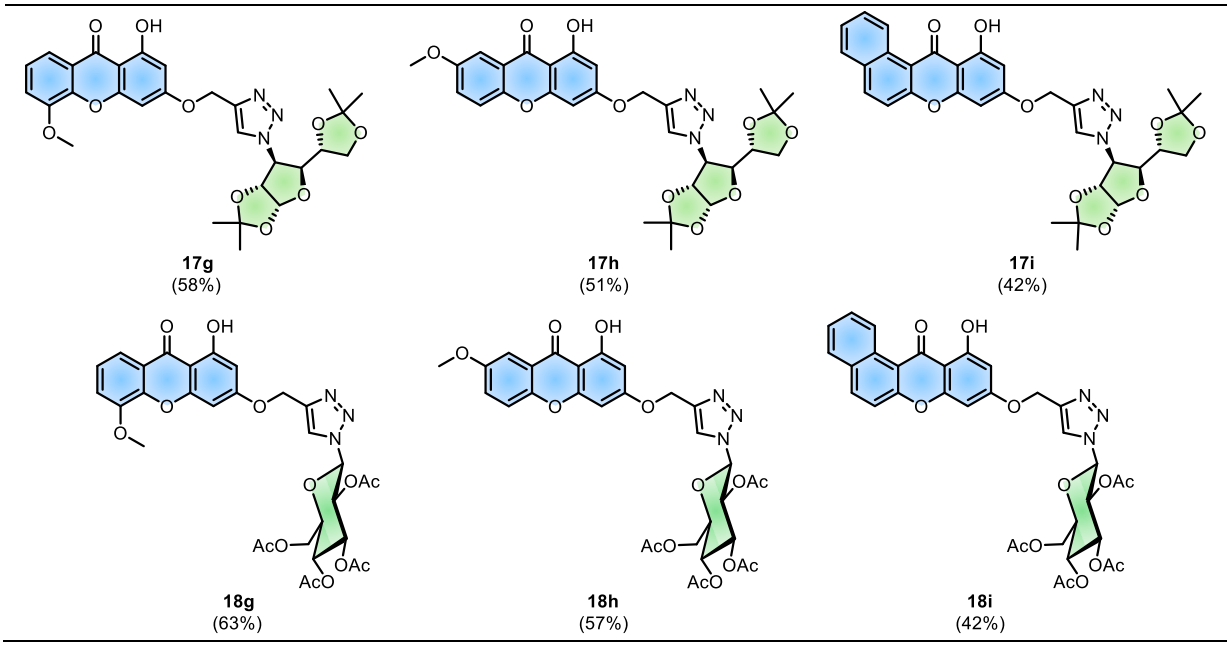

predicting the binding mode (conformation and orientation) of xanthones into α-glucosidase. First, we identified the plausible cavity where ligands interact with amino acid residues using the Glide software (extra precision algorithm) [43,44], and the α-glucosidase was obtained from the AlphaFold Protein Structure Database using the Uniprot identification P38158 [11]. A preliminary screening provided relevant information: compounds bound to the allosteric site formed by Phe157, His239, His279, and Arg312 –the active site is located at Asp214, Glu276, and Asp349– [16] (Fig. S1), which explains the non-competitive or mixed inhibition detected in the Lineweaver-Burk plots (Fig. 6).

A deeper *in silico* analysis suggests that compounds are stabilized by π-π stacking between the xanthone core and His239/His279 (Fig. 8A and C), which may explain the remarkable activity of linear benzoxanthones (Figs. 8C and 4). In some cases, the triazole ring also interacts with these residues. Furthermore, the oxygen atom of the xanthone forms a hydrogen bond with Asn241, an amino acid that also interacts with heteroatoms of the triazole ring or the carbohydrate moiety (Fig. 8B and C). Finally, we recognized another meaningful interaction: Arg312 forms a hydrogen bond with the carbonyl or hydroxyl groups of the xanthone cycle (Table 3).

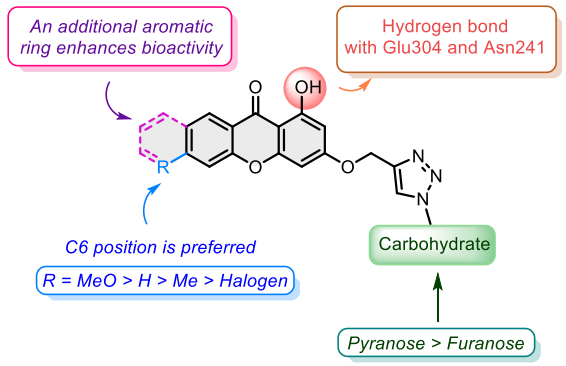

Fig. 5. Structure-Activity Relationship (SAR) xanthone-carbohydrate hybrids **17** and **18**.

When comparing the docking molecular results of triazole-furanose/pyranose derivatives with compound **4a** [16], we observed that both interact with the same allosteric site residues (Fig. 8D and Table 3); Nevertheless, the binding mode of compound **4a** differs from that of the designed compounds, which is reflected in their docking score (Table 3). While **4a** displays a docking score of −5.11 (the most active compound in a previous work) [16], the xanthone-furanose/pyranose hybrids exhibit lower energy values (compound **17f** showed the highest affinity with −7.35), indicating a noteworthy stability for the ligand-receptor complex.

As an additional approach to evaluating the reliability of the binding mode obtained from molecular docking, we performed unrestrained molecular dynamics simulations for the complex between the α-glucosidase and compound **17f** (Fig. 9). The study consisted of five independent replicas, each 100 ns in duration. A putative ligand pose that remains bound to the protein throughout all simulation replicas is considered to have a high probability of being correct [45,46]. As shown in Fig. 8, compound **17f** not only remained firmly associated with the allosteric site of the enzyme but also preserved nearly the same binding conformation, indicating a highly favorable interaction between the two molecules. Most of the amino acids involved in the **17f**-glucosidase complex continued interacting with the xanthone in at least 80 % of the simulation (blue-marked amino acids, Fig. 8A and Table S6). Besides, the hydroxy group of C1 established a hydrogen bond with Glu304 during most of the simulation (40 %, Table S7); the remaining time, a second hydrogen bond with Asn241 (26 %) stabilized the complex (interaction detected in other xanthones, Table 3). Finally, the root mean square fluctuation (RMSF, Fig. S2) revealed that only two atoms (methyl groups of the exocyclic acetonide) exhibited significant deviations; these groups had no interaction with amino acids and were exposed to the solvent, which corroborated the computational findings.

3. Conclusions

To enhance the therapeutic arsenal against T2DM, we designed and synthesized two series of xanthone-furanose/pyranose hybrids as potential α-glucosidase inhibitors. The construction of these molecules involved a key regioselective alkylation and a *click* chemistry reaction (CuAAC process). All compounds showed an interesting inhibitory activity against yeast α-glucosidase (ranging from 58.6 to 97.5 %); the benzoxanthones **17f** and **18f**, as well as the methoxylated analog **18c**, became the most remarkable compounds with a lower IC_{50} value than acarbose (7.3 ± 0.3 mM). Enzymatic studies demonstrated that these compounds act as non-competitive or mixed inhibitors for this hydrolase, which agrees with *in silico* studies: xanthones bind into the proposed allosteric site. The complex involving **17f** and α-glucosidase exhibited minimal conformational changes during a 100-ns molecular dynamics simulation.

Furthermore, the compounds exhibited insignificant toxicity in the *Artemia salina* model and moderate cytotoxicity in the COS-7 healthy cell line. Finally, the oral sucrose tolerance test suggests α-glucosidase inhibition as the potential mechanism of action of these xanthone-containing hybrids, since, in normoglycemic mice, benzoxanthones

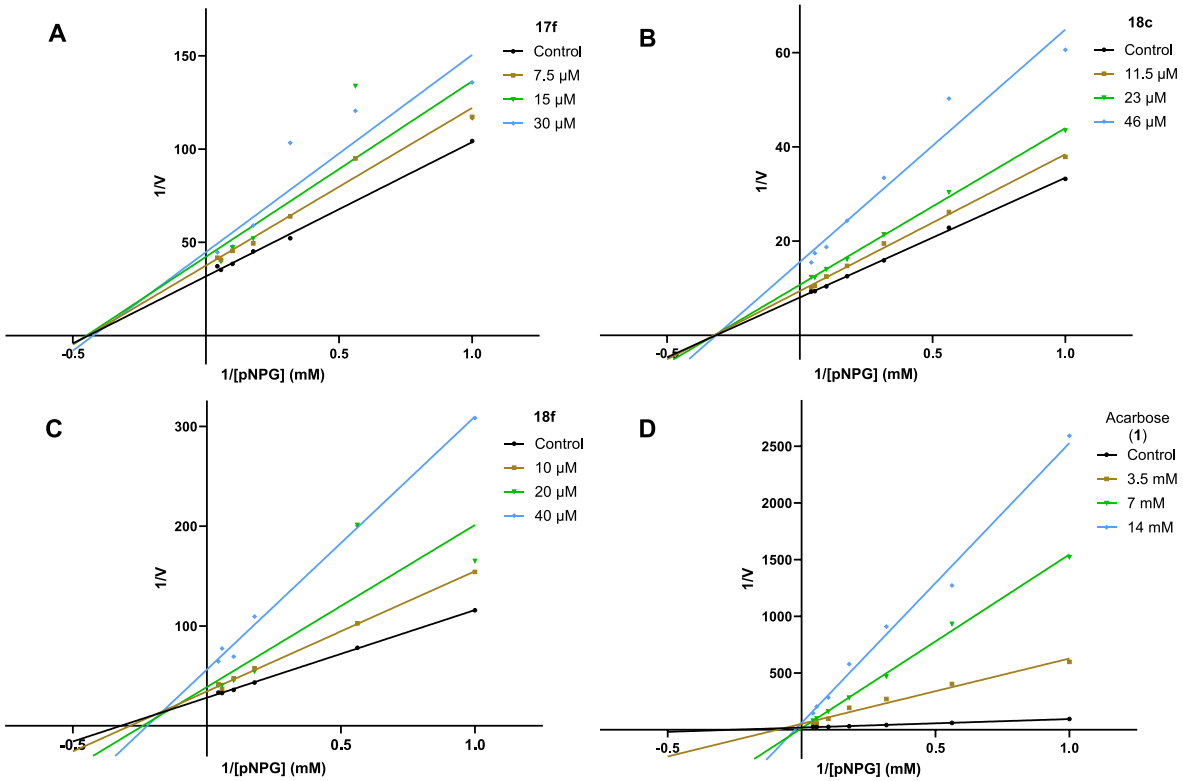

Fig. 6. Lineweaver-Burk plots for α-glucosidase inhibition of xanthones **17f**, **18c**, and **18f** and acarbose (control). ½ x IC_{50}, IC_{50} and 2 x IC_{50} were tested.

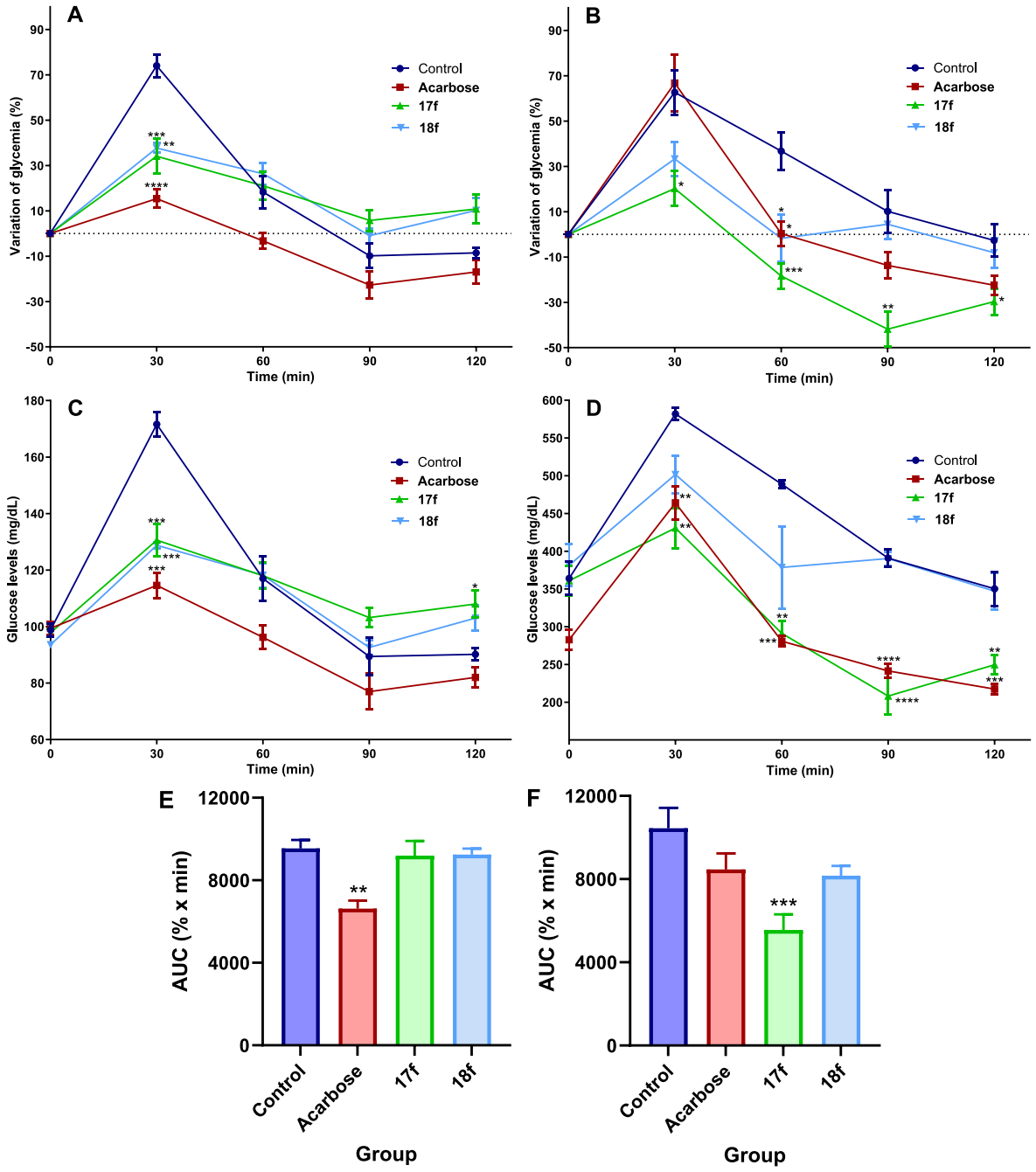

Fig. 7. Glycemia variation after treatment with acarbose (**1**) and compounds **17f** and **18f** on: A) Normoglycemic mice; B) STZ-induced diabetic mice. Similarly, glucose levels after treatment indicate the anti-hyperglycemic effect of the tested compounds on: C) Normoglycemic mice; D) STZ-induced diabetic mice. E) AUC for normoglycemic mice; F) AUC for diabetic mice. Mean ± SEM (n = 5). Significant difference vs. the control group: $^{*}p \leq 0.05$; $^{**}p \leq 0.01$; $^{***}p \leq 0.001$; $^{****}p \leq 0.0001$.

17f and **18f** diminished considerably the glycemia peak after sucrose administration (34.1 ± 7.6 % and 37.7 ± 2.2 %, respectively), in comparison with the control group (74.0 ± 5.1 %; acarbose had a 15.4 ± 4.1 %% of reduction). We want to emphasize the notable anti-hyperglycemic effect of the hybrid **17f** at 120 min (lower glucose levels than the control group), suggesting an additional biological activity. Future studies will focus on elucidating the entire mechanism of action of these hybrids, which, surely enough, become interesting candidates for further optimization.

4. Experimental section

4.1. General

Reagents and solvents were acquired from Sigma Aldrich and Química Rique. The advance of the reactions was monitored by TLC and UV light. ^{1}H and ^{13}C NMR spectra were recorded with Jeol Eclipse 300 MHz and Jeol ECZ400S 400 MHz, using $CDCl_3$ and DMSO-d_6. High-resolution mass spectra (HRMS) were measured using a Jeol JMS-T100LC The AccuTOF mass spectrometer with DART (Direct Analysis in Real Time) ionization technique. Infrared (IR) spectra were collected with a Thermo Fisher Scientific model Nicolet iS50 FT-IR spectrometer using the ATR

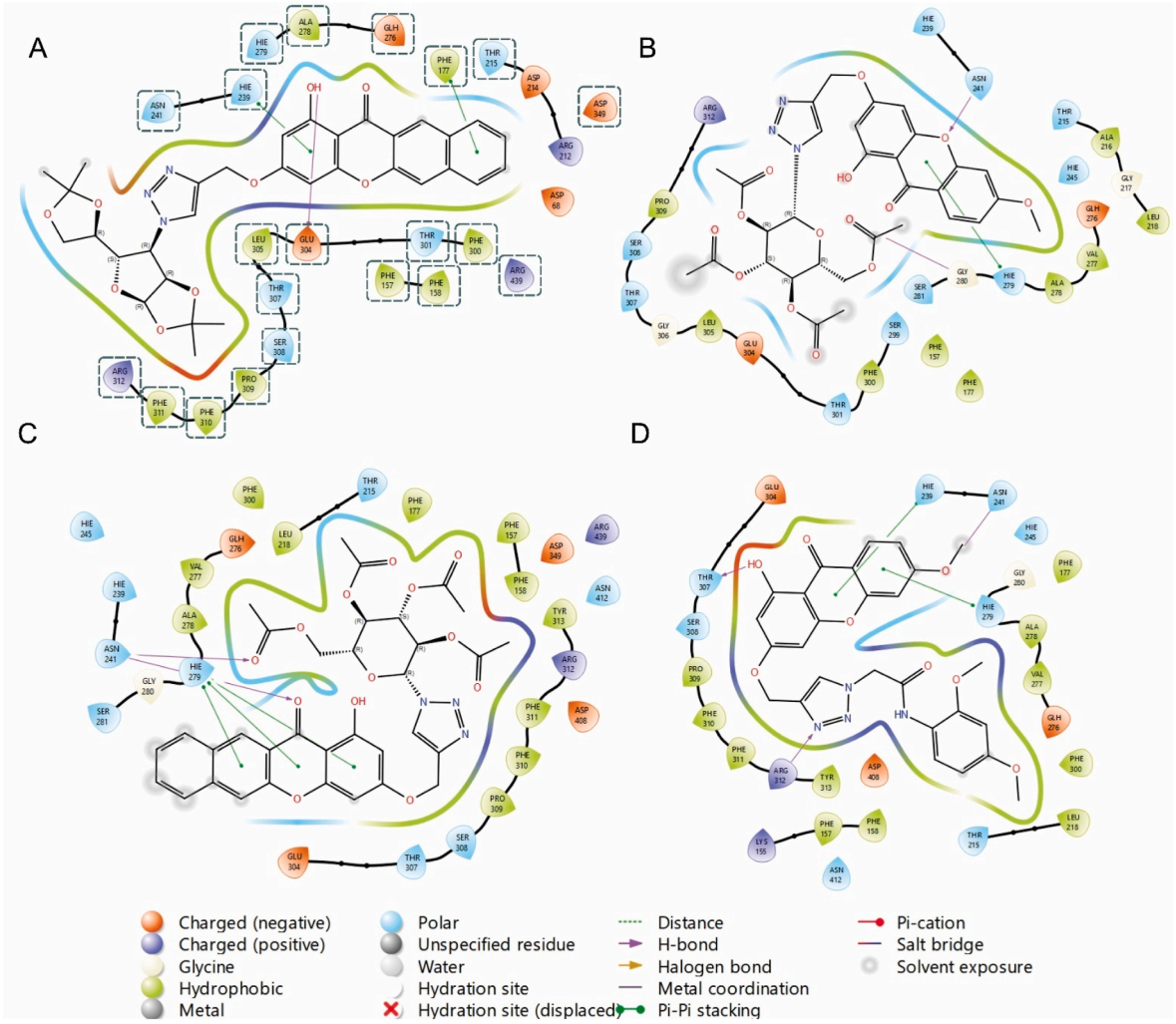

Fig. 8. Two-dimensional plot for: A) **17f**; B) **18c**; C) **18f**; and D) **4a**. In the case of **17f**, blue boxes indicate those amino acids that interacted with the ligand with a 0.8 frequency after molecular dynamics simulation (100 ns). (For interpretation of the references to colour in this figure legend, the reader is referred to the Web version of this article.)

(Attenuated Total Reflection) technique.

4.2. General procedure for the synthesis of 9H-xanthen-9-one (14a-i)

In a round-bottom flask attached to a Vigreux column, the corresponding salicylic acid (100 mg, 724 μmol) and phloroglucinol (100 mg, 869 μmol) were dissolved in 1.33 mL of Eaton's reagent (P_2O_5–CH_3SO_3H). The mixture was stirred for 3 h at 80 °C, then cooled to room temperature. Subsequently, cold water was added, and an orange-brown solid precipitated immediately. After vigorous stirring for 2 h, the solid was collected by filtration and washed with water. To remove phosphorus salts, the recovered solid was purified by flash column chromatography (Hex-AcOEt as the eluent), affording the desired xanthone.

4.3. General procedure for the propargylation of xanthones (16a-i)

In a round-bottom flask, the corresponding xanthone **14** (100 mg, 438 μmol) and potassium carbonate (182 mg, 1.31 mmol) were suspended in MeCN (4.4 mL). The mixture was allowed to react for 30 min at 60 °C until the formation of a yellow solid; then, a propargyl bromide solution 80 wt % in toluene (78.2 mg, 526 μmol) was added dropwise and stirred for 3–12 h at 60 °C. Afterward, the excess solvent was removed by evaporation under reduced pressure. The solid was redissolved in AcOEt and acidified with a 1 M HCl solution. The organic phase was dried with Na_2SO_4 and evaporated under reduced pressure. Finally, the desired product was isolated by flash column chromatography (Hex-AcOEt as the eluent).

4.3.1. 1-Hydroxy-3-(prop-2-yn-1-yloxy)-9H-xanthen-9-one (16a)

Obtained as a white solid after flash chromatography purification (Hex-AcOEt 8:2) in 59 % yield. **^{1}H-NMR** (400 MHz, DMSO-d_6) δ: 12.76 (s, 1H), 8.12 (dd, J = 8.0 and 1.6 Hz, 1H), 7.87 (ddd, J = 8.6, 7.2, and 1.6 Hz, 1H), 7.60 (dd, J = 8.4 and 0.8 Hz, 1H), 7.47 (ddd, J = 8.0, 6.8, and 0.8 Hz, 1H), 6.67 (d, J = 2.4 Hz, 1H), 6.44 (d, J = 2.4 Hz, 1H), 4.97 (d, J = 2.4 Hz, 2H), 3.69 (t, J = 2.4 Hz, 1H); **^{13}C-NMR** (100 MHz, DMSO-d_6) δ: 180.8, 164.9, 163.1, 157.6, 156.0, 136.5, 125.8, 125.1, 120.3, 118.3, 104.0, 98.3, 94.2, 79.7, 78.8, 56.9; **MS** (DART+) m/z: $[M+H]^+$; 267; **HRMS** m/z calcd for $^{12}C^1_{16}H^{16}_{11}O_4$ $[M+H]^+$, 267.06573; found 267.06568.

4.3.2. 1-Hydroxy-6-methyl-3-(prop-2-yn-1-yloxy)-9H-xanthen-9-one (16b)

Obtained as a white solid after flash chromatography purification (Hex-AcOEt 9:1) in 51 % yield. **^{1}H-NMR** (400 MHz, $CDCl_3$) δ: 12.87 (s, 1H), 8.04 (d, J = 8.0 Hz, 1H), 7.174–7.167 (comp, 1H), 7.14–7.12 (comp, 1H), 6.44 (d, J = 2.4 Hz, 1H), 6.34 (d, J = 2.4 Hz, 1H), 4.72 (d, J = 2.4 Hz, 2H), 2.58 (t, J = 2.4 Hz, 1H), 2.45 (s, 3H); **^{13}C-NMR** (100 MHz,

Table 3
Docking results of xanthone-containing compounds.

Compound	Docking score	Interactions				
		His239	Asn241	His279	Arg312	Others
4a	−5.11	✓	✓	✓	✓	Thr307
17a	−6.87	–	✓	✓	–	Glu304
17b	−6.25	–	–	–	✓	Phe300
17c	−6.45	–	✓	✓	–	–
17d	−5.54	–	–	–	✓	Pro309
17e	−6.92	✓	✓	✓	–	Glu276
17f	**−7.35**	✓	–	–	–	Phe177, Glu304
17g	−5.83	✓	✓[a]	–	–	Phe300
17h	−5.98	–	–	–	–	Arg439
17i	−5.56	–	–	–	–	Asp408
18a	−1.23	–	–	–	–	Phe177, Glu304
18b	−6.39	–	✓	✓	–	Ser281[a], Glu304
18c	−5.24	–	✓	✓	–	Gly280[a]
18d	−4.05	–	✓[a]	–	✓	Gly280
18e	−6.45	✓[a]	–	✓	–	Asp214, Glu276
18f	−6.14	–	✓[a]	✓	–	–
18g	−1.69	✓[a]	✓	✓	✓[a]	–
18h	−1.50	✓	✓	–	✓[a]	–
18i	−3.19	–	–	–	–	Phe157

[a] Residue interacts with carbohydrates.

$CDCl_3$) δ: 180.8, 164.3, 163.5, 157.6, 156.2, 146.9, 125.7, 125.6, 118.3, 117.5, 104.3, 97.7, 93.6, 77.4, 76.7, 56.2, 22.1; **MS** (DART+) *m/z*: $[M+H]^+$; 281; **HRMS** *m/z* calcd for $^{12}C_{17}^{1}H_{13}^{16}O_4$ $[M+H]^+$, 281.08138; found 281.08146.

4.3.3. 1-Hydroxy-6-methoxy-3-(prop-2-yn-1-yloxy)-9H-xanthen-9-one (16c)

Obtained as a white solid after flash chromatography purification (Hex-AcOEt 85:15) in 54 % yield. **^{1}H-NMR** (300 MHz, $CDCl_3$) δ: 13.00 (s, 1H), 8.14 (d, *J* = 9.0 Hz, 1H), 6.94 (dd, *J* = 9.0 and 2.4 Hz, 1H), 6.84 (d, *J* = 2.4 Hz, 1H), 6.48 (d, *J* = 2.4 Hz, 1H), 6.41 (d, *J* = 2.4 Hz, 1H), 4.77 (d, *J* = 2.4 Hz, 2H), 3.93 (s, 3H), 2.60 (t, *J* = 2.4 Hz, 1H); **^{13}C-NMR** (100 MHz, $CDCl_3$) δ: 180.3, 165.5, 164.1, 163.6, 158.1, 157.7, 127.5, 114.4, 113.4, 104.2, 100.3, 97.8, 93.7, 77.5, 76.6, 56.3, 56.0; **MS** (DART+) *m/z*: $[M+H]^+$; 297; **HRMS** *m/z* calcd for $^{12}C_{17}^{1}H_{13}^{16}O_5$ $[M+H]^+$, 297.07630; found 297.07643.

4.3.4. 1-Hydroxy-6-fluoro-3-(prop-2-yn-1-yloxy)-9H-xanthen-9-one (16d)

Obtained as a white solid after flash chromatography purification (Hex-AcOEt 85:15) in 69 % yield. **^{1}H-NMR** (300 MHz, $CDCl_3$) δ: 12.76 (s, 1H), 8.29–8.24 (comp, 1H), 7.14–7.08 (comp, 2H), 6.52 (d, *J* = 2.4 Hz, 1H), 6.45 (d, *J* = 2.4 Hz, 1H), 4.78 (d, *J* = 2.4 Hz, 2H), 2.61 (t, *J* = 2.4 Hz, 1H); **^{13}C-NMR** (75 MHz, $CDCl_3$) δ: 180.1, 166.8 (d, *J* = 255.0 Hz), 164.6, 163.7, 157.8, 157.3 (d, *J* = 14.0 Hz), 128.6 (d, *J* = 11.3 Hz), 117.6 (d, *J* = 2.0 Hz), 113.0 (d, *J* = 22.5 Hz), 104.6 (d, *J* = 25.5 Hz), 104.2, 98.2, 93.9, 77.3, 76.8, 56.3; **MS** (DART+) *m/z*: $[M+H]^+$; 285; **HRMS** *m/z* calcd for $^{12}C_{16}^{1}H_{10}^{19}F_1^{16}O_4$ $[M+H]^+$, 285.05631; found 285.05635.

4.3.5. 5,7-Dichloro-1-hydroxy-3-(prop-2-yn-1-yloxy)-9H-xanthen-9-one (16e)

Obtained as a yellowish solid after flash chromatography purification (Hex-AcOEt 85:15) in 75 % yield. **^{1}H-NMR** (300 MHz, $CDCl_3$ and DMSO-d_6) δ: 12.31 (s, 1H), 7.97 (d, *J* = 2.4 Hz, 1H), 7.64 (d, *J* = 2.4 Hz, 1H), 6.50 (d, *J* = 2.4 Hz, 1H), 6.33 (d, *J* = 2.4 Hz, 1H), 4.68 (d, *J* = 2.4 Hz, 2H), 2.57 (t, *J* = 2.4 Hz, 1H); **MS** (DART+) *m/z*: $[M+H]^+$; 335; **HRMS** *m/z* calcd for $^{12}C_{16}^{1}H_9^{35}Cl_2^{16}O_4$ $[M+H]^+$, 334.98779; found 334.98777.

4.3.6. 1-Hydroxy-3-(prop-2-yn-1-yloxy)-12h-benzo[b]xanthen-12-one (16f)

Obtained as a yellow solid after flash chromatography purification (Hex-AcOEt 8:2) in 75 % yield. **^{1}H-NMR** (400 MHz, $CDCl_3$ and DMSO-d_6) δ: 12.89 (s, 1H), 8.80 (s, 1H), 8.02 (d, *J* = 8.4 Hz, 1H), 7.87 (d, *J* = 8.4 Hz, 1H), 7.60 (ddd, *J* = 8.4, 6.8, and 1.2 Hz, 1H), 7.48 (ddd, *J* = 8.0, 6.8, and 1.2 Hz, 1H), 6.50 (d, *J* = 2.4 Hz, 1H), 6.38 (d, *J* = 2.4 Hz, 1H), 4.77 (d, *J* = 2.4 Hz, 2H), 2.61 (t, *J* = 2.4 Hz, 1H); **^{13}C-NMR** (100 MHz, $CDCl_3$ and DMSO-d_6) δ: 181.6, 165.1, 164.1, 158.1, 152.0, 136.9, 129.8, 129.7, 129.4, 127.7, 127.2, 125.8, 120.2, 113.4, 103.8, 97.4, 94.0, 77.4, 76.7, 56.3; **MS** (DART+) *m/z*: $[M+H]^+$; 317; **HRMS** *m/z*

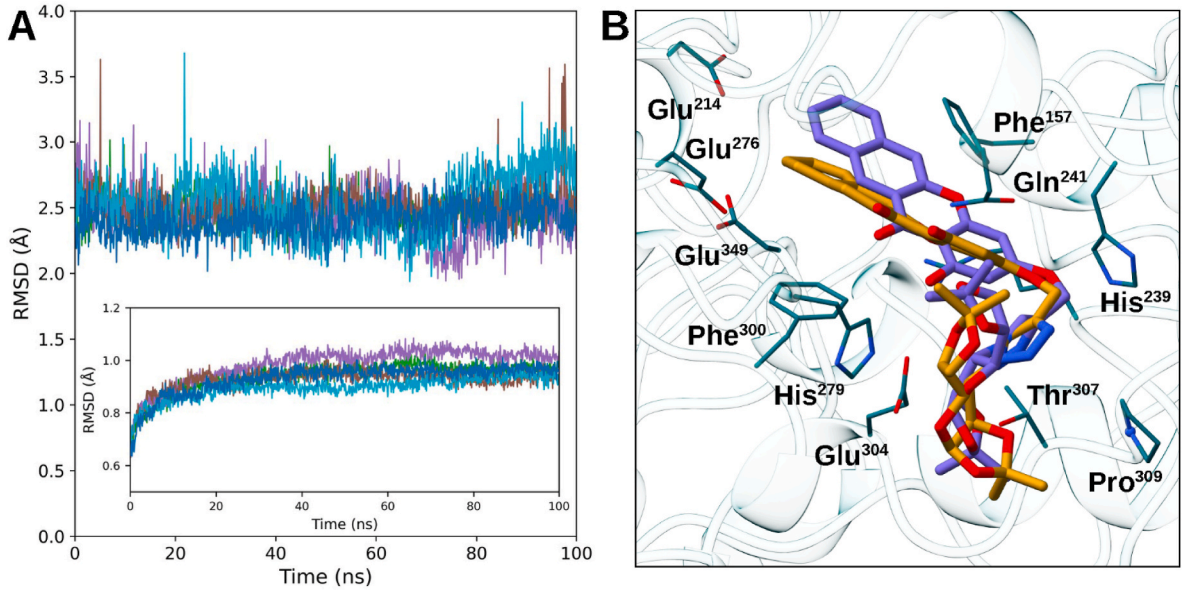

Fig. 9. Evaluation of the binding pose stability of compound **17f** through molecular dynamics simulations. A) Time evolution of the ligand RMSD with respect to the original docked pose. The inset displays the corresponding RMSD values for the enzyme backbone atoms. B) Comparison between the dominant ligand conformer (orange sticks), representing ~40 % of the simulation time, and the initial docked pose (purple sticks). Five independent 100-ns replicas were performed at 310 K and pH 6.8. (For interpretation of the references to colour in this figure legend, the reader is referred to the Web version of this article.)

calcd for $^{12}C^{1}_{20}H^{16}_{13}O_4$ $[M+H]^+$, 317.08138; found 317.08154.

4.3.7. 1-Hydroxy-5-methoxy-3-(prop-2-yn-1-yloxy)-9H-xanthen-9-one (16g)

Obtained as a white solid after flash chromatography purification (Hex-AcOEt 7:3) in 75 % yield. **^{1}H-NMR** (400 MHz, $CDCl_3$ and DMSO-d_6) δ: 12.81 (s, 1H), 7.80 (dd, J = 7.6 and 1.6 Hz, 1H), 7.29 (t, J = 8.0 Hz, 1H), 7.23 (dd, J = 8.0 and 1.6 Hz, 1H), 6.62 (d, J = 2.4 Hz, 1H), 6.41 (d, J = 2.4 Hz, 1H), 4.75 (d, J = 2.4 Hz, 2H), 4.01 (s, 3H), 2.58 (t, J = 2.4 Hz, 1H); **^{13}C-NMR** (100 MHz, $CDCl_3$ and DMSO-d_6) δ: 181.0, 164.6, 163.4, 157.5, 148.4, 146.4, 123.8, 121.6, 116.8, 115.9, 104.5, 98.3, 93.7, 77.3, 76.7, 56.5, 56.3; **MS** (DART+) *m/z*: $[M+H]^+$; 297; **HRMS** *m/z* calcd for $^{12}C^{1}_{17}H^{16}_{13}O_5$ $[M+H]^+$, 297.07630; found 297.07618.

4.3.8. 1-Hydroxy-7-methoxy-3-(prop-2-yn-1-yloxy)-9H-xanthen-9-one (16h)

Obtained as a yellow solid after flash chromatography purification (Hex-AcOEt 8:2) in 70 % yield. **^{1}H-NMR** (400 MHz, $CDCl_3$) δ: 12.88 (s, 1H), 7.62 (d, J = 2.8 Hz, 1H), 7.39 (d, J = 9.2 Hz, 1H), 7.32 (dd, J = 9.2 and 2.8 Hz, 1H), 6.52 (d, J = 2.4 Hz, 1H), 6.43 (d, J = 2.4 Hz, 1H), 4.78 (d, J = 2.4 Hz, 2H), 3.92 (s, 3H), 2.60 (t, J = 2.4 Hz, 1H); **^{13}C-NMR** (75 MHz, $CDCl_3$) δ: 180.9, 164.4, 163.5, 157.8, 156.2, 151.0, 125.2, 119.2, 114.3, 105.3, 104.3, 97.8, 93.5, 77.3, 76.6, 56.3, 56.1; **MS** (EI+) *m/z*: $[M]^+$; 296; **HRMS** *m/z* calcd for $^{12}C^{1}_{17}H^{16}_{12}O_5$ $[M+H]^+$, 296.0685; found 296.0680.

4.3.9. 11-Hydroxy-9-(prop-2-yn-1-yloxy)-12h-benzo[a]xanthen-12-one (16i)

Obtained as a yellow solid after flash chromatography purification (Hex-AcOEt 85:15) in 84 % yield. **^{1}H-NMR** (400 MHz, $CDCl_3$) δ: 13.47 (s, 1H), 9.95 (d, J = 8.8 Hz, 1H), 8.13 (d, J = 8.8 Hz, 1H), 7.91 (d, J = 8.0 Hz, 1H), 7.77 (ddd, J = 8.4, 6.8, and 1.2 Hz, 1H), 7.61 (ddd, J = 8.0, 6.8, and 1.2 Hz, 1H), 7.51 (d, J = 9.2 Hz, 1H), 6.57 (d, J = 2.4 Hz, 1H), 6.48 (d, J = 2.4 Hz, 1H), 4.79 (d, J = 2.4 Hz, 2H), 2.61 (t, J = 2.4 Hz, 1H); **^{13}C-NMR** (100 MHz, $CDCl_3$) δ: 183.2, 163.7, 163.6, 157.8, 156.5, 137.2, 130.9, 130.3, 129.7, 128.7, 126.9, 126.4, 117.7, 113.4, 105.8, 98.4, 93.0, 77.5, 76.6, 56.3; **MS** (DART+) *m/z*: $[M+H]^+$; 317; **HRMS** *m/z* calcd for $^{12}C^{1}_{20}H^{16}_{13}O_4$ $[M+H]^+$, 317.08138; found 317.08146.

4.4. General procedure for the synthesis of azide-carbohydrates

Azide-containing furanose was prepared following the methodology by Nagy et al. [18] While azido-pyranose was synthesized according to a previously reported method [19].

4.4.1. (3aR,5S,6S,6aR)-6-azido-5-((R)-2,2-dimethyl-1,3-dioxolan-4-yl)-2,2-dimethyltetrahydrofuro[2,3-d] [1,3]dioxole (9)

^{1}H-NMR (500 MHz, $CDCl_3$) δ: 5.81 (d, J = 4.0 Hz, 1H), 4.61 (dd, J = 5.5 and 4.0, 1H), 4.30 (td, J = 6.5 and 5.0 Hz, 1H), 4.08 (dd, J = 8.5 and 6.5 Hz, 1H), 4.06–4.02 (comp, 1H), 4.01 (dd, J = 8.5 and 6.5 Hz, 1H), 3.81 (dd, J = 8.5 and 5.0 Hz, 1H), 1.57 (s, 3H), 1.46 (s, 3H), 1.38 (s, 3H), 1.37 (s, 3H); **^{13}C-NMR** (125 MHz, $CDCl_3$) δ: 112.8, 109.8, 104.0, 79.8, 79.0, 75.6, 72.5, 65.9, 26.6, 26.5, 26.3, 25.3.

4.4.2. (2R,3R,4S,5R,6R)-2-(acetoxymethyl)-6-azidotetrahydro-2H-pyran-3,4,5-triyl triacetate (11)

^{1}H-NMR (500 MHz, $CDCl_3$) δ: 5.22 (t, J = 9.5 Hz, 1H), 5.11 (dd, J = 10.0 and 9.5 Hz, 1H), 4.96 (dd, J = 9.5 and 9.0 Hz, 1H), 4.66 (d, J = 9.0 Hz, 1H), 4.28 (dd, J = 12.5 and 5.0 Hz, 1H), 4.18 (dd, J = 12.5 and 2.0 Hz, 1H), 3.81 (ddd, J = 10.0, 5.0, and 2.0 Hz, 1H), 2.10 (s, 3H), 2.08 (s, 3H), 2.03 (s, 3H), 2.01 (s, 3H); **^{13}C-NMR** (125 MHz, $CDCl_3$) δ: 170.5, 170.0, 169.2, 169.1, 87.9, 74.0, 72.6, 70.6, 67.9, 61.6, 20.6, 20.48, 20.46 (2C).

4.5. General procedure for the synthesis of xanthone-triazol-carbohydrate (17a-i and 18a-i)

In a round-bottom flask, the corresponding propargylxanthone **16** (20 mg, 75 μmol), azide-carbohydrate **9** or **11** (26 mg, 90 μmol), sodium L-ascorbate (3 mg, 15 μmol), and copper(II) sulfate pentahydrate (2.4 mg, 15 μmol) were dissolved in DMSO (100 μL). The resulting mixture was stirred overnight at room temperature. Next, the reaction was treated with water to precipitate the product, which was collected by filtration and purified by flash column chromatography (Hex-AcOEt as the eluent), providing the desired triazole.

4.5.1. 3-((1-((3aR,5S,6S,6aR)-5-((R)-2,2-dimethyl-1,3-dioxolan-4-yl)-2,2-dimethyltetrahydrofuro[2,3-d] [1,3]dioxol-6-yl)-1H-1,2,3-triazol-4-yl) methoxy)-1-hydroxy-9H-xanthen-9-one (17a)

Obtained as a yellowish solid after flash chromatography purification (Hex-AcOEt 7:3) in 52 % yield. **^{1}H-NMR** (400 MHz, $CDCl_3$) δ: 12.84 (s, 1H), 8.24 (dd, J = 8.0 and 1.6 Hz, 1H), 7.82 (s, 1H), 7.71 (ddd, J = 8.4, 7.1, and 1.7 Hz, 1H), 7.43 (dd, J = 8.4 and 0.8 Hz, 1H), 7.37 (ddd, J = 8.4, 7.1, and 1.7 Hz, 1H), 6.53 (d, J = 2.4 Hz, 1H), 6.40 (d, J = 2.4 Hz, 1H), 6.26 (d, J = 3.6 Hz, 1H), 5.31 (s, 2H), 5.21 (d, J = 3.2 Hz, 1H), 5.02 (d, J = 3.6 Hz, 1H), 4.33 (dd, J = 9.6 and 4.0 Hz, 1H), 3.93 (d, J = 3.6 Hz, 1H), 3.92 (d, J = 2.4 Hz, 1H), 3.09 (dt, J = 9.2 and 5.2 Hz, 1H), 1.59 (s, 3H), 1.43 (s, 3H), 1.37 (s, 3H), 1.17 (s, 3H); **^{13}C-NMR** (100 MHz, $CDCl_3$) δ: 181.0, 165.2, 163.6, 157.8, 156.1, 142.8, 135.2, 126.0, 125.2, 124.2, 120.7, 117.7, 112.7, 109.9, 106.4, 104.4, 97.9, 93.5, 83.5, 80.6, 72.4, 67.7, 66.0, 62.4, 27.0, 26.8, 26.2, 25.0; **MS** (DART+) *m/z*: $[M+H]^+$; 552; **HRMS** *m/z* calcd for $^{12}C^{1}_{28}H^{14}_{30}N^{16}_{3}O_9$ $[M+H]^+$, 552.19820; found 552.19844; **IR** (ATR, cm^{-1}): 3139, 3089, 2990, 2922, 2893, 2852, 1655, 1648, 1608, 1569, 1487, 1467, 1205, 1151, 1076, 1059, 1020, 825.

4.5.2. 3-((1-((3aR,5S,6S,6aR)-5-((R)-2,2-dimethyl-1,3-dioxolan-4-yl)-2,2-dimethyltetrahydrofuro[2,3-d] [1,3]dioxol-6-yl)-1H-1,2,3-triazol-4-yl) methoxy)-1-hydroxy-6-methyl-9H-xanthen-9-one (17b)

Obtained as a yellowish solid after flash chromatography purification (Hex-AcOEt 7:3) in 50 % yield. **^{1}H-NMR** (400 MHz, $CDCl_3$) δ: 12.90 (s, 1H), 8.10 (d, J = 8.0 Hz, 1H), 7.81 (s, 1H), 7.211–7.204 (comp, 1H), 7.19–7.16 (comp, 1H), 6.50 (d, J = 2.4 Hz, 1H), 6.38 (d, J = 2.4 Hz, 1H), 6.26 (d, J = 3.6 Hz, 1H), 5.30 (s, 2H), 5.21 (d, J = 3.6 Hz, 1H), 5.01 (d, J = 3.6 Hz, 1H), 4.33 (dd, J = 9.6 and 3.6 Hz, 1H), 3.93 (d, J = 3.2 Hz, 1H), 3.92 (d, J = 2.4 Hz, 1H), 3.09 (dt, J = 9.6 and 5.6 Hz, 1H), 2.49 (s, 3H), 1.58 (s, 3H), 1.43 (s, 3H), 1.37 (s, 3H), 1.16 (s, 3H); **^{13}C-NMR** (100 MHz, $CDCl_3$) δ: 180.8, 165.0, 163.6, 157.8, 156.2, 146.9, 142.8, 125.7, 125.2, 118.4, 117.5, 112.7, 109.9, 106.4, 104.3, 97.8, 93.4, 83.5, 80.6, 72.3, 67.7, 66.0, 62.4, 27.0, 26.8, 26.2, 25.0, 22.1; **MS** (DART+) *m/z*: $[M+H]^+$; 566; **HRMS** *m/z* calcd for $^{12}C^{1}_{29}H^{14}_{32}N^{16}_{3}O_9$ $[M+H]^+$, 566.21385; found 566.21386; **IR** (ATR, cm^{-1}): 3080, 2993, 2934, 2878, 1649, 1600, 1566, 1501, 1452, 1210, 1168, 1077, 1035, 1014, 788.

4.5.3. 3-((1-((3aR,5S,6S,6aR)-5-((R)-2,2-dimethyl-1,3-dioxolan-4-yl)-2,2-dimethyltetrahydrofuro[2,3-d] [1,3]dioxol-6-yl)-1H-1,2,3-triazol-4-yl) methoxy)-1-hydroxy-6-methoxy-9H-xanthen-9-one (17c)

Obtained as a yellowish solid after flash chromatography purification (Hex-AcOEt 7:3) in 51 % yield. **^{1}H-NMR** (400 MHz, $CDCl_3$) δ: 12.96 (s, 1H), 8.11 (d, J = 8.8 Hz, 1H), 7.81 (s, 1H), 6.92 (dd, J = 8.8 and 2.4 Hz, 1H), 6.81 (d, J = 2.0 Hz, 1H), 6.47 (d, J = 2.4 Hz, 1H), 6.37 (d, J = 2.4 Hz, 1H), 6.25 (d, J = 3.2 Hz, 1H), 5.29 (s, 2H), 5.21 (d, J = 3.2 Hz, 1H), 5.01 (d, J = 3.6 Hz, 1H), 4.33 (dd, J = 9.2 and 3.6 Hz, 1H), 3.94–3.92 (comp, 2H), 3.92 (s, 3H), 3.09 (dt, J = 9.6 and 5.2 Hz, 1H), 1.58 (s, 3H), 1.43 (s, 3H), 1.37 (s, 3H), 1.16 (s, 3H); **^{13}C-NMR** (100 MHz, $CDCl_3$) δ: 180.2, 165.5, 164.7, 163.6, 158.1, 157.8, 142.8, 127.4, 125.2, 114.3, 113.4, 112.7, 109.9, 106.4, 104.0, 100.2, 97.9, 93.4, 83.5, 80.6, 72.3, 67.7, 66.0, 62.3, 56.0, 27.0, 26.8, 26.2, 25.0; **MS** (DART+) *m/z*: $[M+H]^+$; 582; **HRMS** *m/z* calcd for $^{12}C^{1}_{29}H^{14}_{32}N^{16}_{3}O_{10}$ $[M+H]^+$, 582.20877; found 582.20894; **IR** (ATR, cm^{-1}): 3079, 2897, 2932, 2850,

1651, 1598, 1570, 1500, 1447, 1263, 1245, 1213, 1168, 1159, 1081, 1067, 1053, 1018, 822, 801.

4.5.4. 3-((1-((3aR,5S,6S,6aR)-5-((R)-2,2-dimethyl-1,3-dioxolan-4-yl)-2,2-dimethyltetrahydrofuro[2,3-d] [1,3]dioxol-6-yl)-1H-1,2,3-triazol-4-yl) methoxy)-1-hydroxy-6-fluoro-9H-xanthen-9-one (17d)

Obtained as a white solid after flash chromatography purification (Hex-AcOEt 8:2) in 50 % yield. **^{1}H-NMR** (400 MHz, $CDCl_3$) δ: 12.73 (s, 1H), 8.27–8.23 (comp, 1H), 7.82 (s, 1H), 7.12–7.08 (comp, 2H), 6.53 (d, J = 2.4 Hz, 1H), 6.42 (d, J = 2.4 Hz, 1H), 6.26 (d, J = 3.6 Hz, 1H), 5.31 (s, 2H), 5.21 (d, J = 3.6 Hz, 1H), 5.02 (d, J = 3.6 Hz, 1H), 4.33 (dd, J = 9.6 and 3.6 Hz, 1H), 3.94 (d, J = 3.6 Hz, 1H), 3.93 (d, J = 2.4 Hz, 1H), 3.09 (dt, J = 9.6 and 5.5 Hz, 1H), 1.59 (s, 3H), 1.43 (s, 3H), 1.38 (s, 3H), 1.17 (s, 3H); **^{13}C-NMR** (100 MHz, $CDCl_3$) δ: 180.0, 166.8 (d, J = 255.0 Hz), 165.2, 163.7, 157.8, 157.4 (d, J = 14.0 Hz), 142.6, 128.6 (d, J = 11.0 Hz), 125.2, 117.6 (d, J = 2.0 Hz), 113.0 (d, J = 23.0 Hz), 112.7, 109.9, 106.4, 104.6 (d, J = 26.0 Hz), 104.0, 98.2, 93.7, 83.5, 80.6, 72.4, 67.7, 66.0, 62.4, 27.0, 26.8, 26.2, 25.0; **MS** (DART+) *m/z*: $[M+H]^+$; 570; **HRMS** *m/z* calcd for $^{12}C^{1}_{28}H^{19}_{29}F^{14}_{1}N^{16}_{3}O_9$ $[M+H]^+$, 570.18878; found 570.18922; **IR** (ATR, cm^{-1}): 3148, 3099, 2990, 2977, 2916, 2849, 1648, 1609, 1499, 1452, 1251, 1195, 1180, 1166, 1067, 1050, 1014, 854, 797.

4.5.5. 5,7-Dichloro-3-((1-((3aR,5S,6S,6aR)-5-((R)-2,2-dimethyl-1,3-dioxolan-4-yl)-2,2-dimethyltetrahydrofuro[2,3-d] [1,3]dioxol-6-yl)-1H-1,2,3-triazol-4-yl)methoxy)-1-hydroxy-9H-xanthen-9-one (17e)

Obtained as a yellow solid after flash chromatography purification (Hex-AcOEt 7:3) in 17 % yield. **^{1}H-NMR** (400 MHz, $CDCl_3$) δ: 12.43 (s, 1H), 8.11 (d, J = 2.4 Hz, 1H), 7.82 (s, 1H), 7.75 (d, J = 2.4 Hz, 1H), 6.64 (d, J = 2.4 Hz, 1H), 6.45 (d, J = 2.4 Hz, 1H), 6.26 (d, J = 3.2 Hz, 1H), 5.33 (s, 2H), 5.22 (d, J = 3.2 Hz, 1H), 5.02 (d, J = 3.6 Hz, 1H), 4.33 (dd, J = 9.2 and 3.6 Hz, 1H), 3.98–3.91 (comp, 2H), 3.10 (dt, J = 9.2 and 5.2 Hz, 1H), 1.59 (s, 3H), 1.44 (s, 3H), 1.38 (s, 3H), 1.18 (s, 3H); **^{13}C-NMR** (100 MHz, $CDCl_3$) δ: 179.1, 165.8, 163.5, 157.3, 150.4, 142.5, 135.0, 129.7, 125.2, 124.1, 123.8, 122.5, 112.7, 109.9, 106.4, 103.9, 98.8, 94.0, 83.5, 80.6, 72.4, 67.7, 66.1, 62.5, 27.0, 26.8, 26.2, 25.0; **MS** (DART+) *m/z*: $[M+H]^+$; 620; **HRMS** *m/z* calcd for $^{12}C^{1}_{28}H^{35}_{28}Cl^{14}_{2}N^{16}_{3}O_9$ $[M+H]^+$, 620.12026; found 620.12028; **IR** (ATR, cm^{-1}): 3075, 2987, 2922, 2872, 2851, 1650, 1621, 1562, 1461, 1201, 1160, 1076, 1051, 1019, 838, 820, 800, 723.

4.5.6. 3-((1-((3aR,5S,6S,6aR)-5-((R)-2,2-dimethyl-1,3-dioxolan-4-yl)-2,2-dimethyltetrahydrofuro[2,3-d] [1,3]dioxol-6-yl)-1H-1,2,3-triazol-4-yl) methoxy)-1-hydroxy-12H-benzo[b]xanthen-12-one (17f)

Obtained as a yellow solid after flash chromatography purification (Hex-AcOEt 8:2) in 41 % yield. **^{1}H-NMR** (400 MHz, $CDCl_3$) δ: 12.90 (s, 1H), 8.81 (s, 1H), 8.03 (d, J = 8.4 Hz, 1H), 7.88 (d, J = 8.0 Hz, 1H), 7.83 (s, 1H), 7.79 (s, 1H), 7.61 (ddd, J = 8.0, 6.8, and 1.2 Hz, 1H), 7.50 (ddd, J = 8.0, 6.8, and 1.2 Hz, 1H), 6.52 (d, J = 2.4 Hz, 1H), 6.38 (d, J = 2.4 Hz, 1H), 6.27 (d, J = 3.2 Hz, 1H), 5.33 (s, 2H), 5.22 (d, J = 3.6 Hz, 1H), 5.02 (d, J = 3.6 Hz, 1H), 4.33 (dd, J = 9.2 and 3.6 Hz, 1H), 3.94 (d, J = 3.6 Hz, 1H), 3.93 (d, J = 3.2 Hz, 1H), 3.11 (dt, J = 9.2 and 5.2 Hz, 1H), 1.59 (s, 3H), 1.44 (s, 3H), 1.38 (s, 3H), 1.18 (s, 3H); **^{13}C-NMR** (100 MHz, $CDCl_3$) δ: 181.5, 165.7, 164.1, 158.3, 151.9, 142.7, 136.9, 129.8, 129.7, 129.4, 127.7, 127.2, 125.8, 125.2, 120.2, 113.3, 112.7, 109.9, 106.5, 103.7, 97.5, 93.7, 83.5, 80.6, 72.4, 67.7, 66.0, 62.4, 27.0, 26.8, 26.3, 25.0; **MS** (DART+) *m/z*: $[M+H]^+$; 602; **HRMS** *m/z* calcd for $^{12}C^{1}_{32}H^{14}_{32}N^{16}_{3}O_9$ $[M+H]^+$, 602.21385; found 602.21387; **IR** (ATR, cm^{-1}): 3323, 3075, 2984, 2927, 2850, 1652, 1612, 1598, 1467, 1450, 1246, 1209, 1178, 1159, 1084, 1018, 816, 748.

4.5.7. 3-((1-((3aR,5S,6S,6aR)-5-((R)-2,2-dimethyl-1,3-dioxolan-4-yl)-2,2-dimethyltetrahydrofuro[2,3-d] [1,3]dioxol-6-yl)-1H-1,2,3-triazol-4-yl) methoxy)-1-hydroxy-5-methoxy-9H-xanthen-9-one (17g)

Obtained as a yellow solid after flash chromatography purification (Hex-AcOEt 6:4) in 58 % yield. **^{1}H-NMR** (400 MHz, $CDCl_3$) δ: 12.80 (s, 1H), 7.81 (s, 1H), 7.78 (dd, J = 7.6 and 1.6 Hz, 1H), 7.28 (t, J = 8.0 Hz, 1H), 7.22 (dd, J = 8.0 and 1.6 Hz, 1H), 6.62 (d, J = 2.4 Hz, 1H), 6.39 (d, J = 2.4 Hz, 1H), 6.25 (d, J = 3.6 Hz, 1H), 5.29 (s, 2H), 5.20 (d, J = 3.6 Hz, 1H), 5.02 (d, J = 4.0 Hz, 1H), 4.32 (dd, J = 9.6 and 4.0 Hz, 1H), 4.01 (s, 3H), 3.97–3.90 (comp, 2H), 3.10 (dt, J = 9.6 and 5.6 Hz, 1H), 1.58 (s, 3H), 1.43 (s, 3H), 1.37 (s, 3H), 1.17 (s, 3H); **^{13}C-NMR** (100 MHz, $CDCl_3$) δ: 180.9, 165.2, 163.4, 157.6, 148.4, 146.4, 142.7, 125.2, 123.8, 121.5, 116.8, 115.8, 112.7, 109.9, 106.4, 104.3, 98.3, 93.4, 83.5, 80.6, 72.3, 67.6, 66.0, 62.4, 56.5, 27.0, 26.8, 26.2, 25.0; **MS** (DART+) *m/z*: $[M+H]^+$; 582; **HRMS** *m/z* calcd for $^{12}C^{1}_{29}H^{14}_{32}N^{16}_{3}O_{10}$ $[M+H]^+$, 582.20877; found 582.20895; **IR** (ATR, cm^{-1}): 3140, 3101, 2985, 2937, 2903, 2851, 1648, 1619, 1609, 1573, 1492, 1443, 1223, 1208, 1158, 1101, 1075, 1017, 800, 728.

4.5.8. 3-((1-((3aR,5S,6S,6aR)-5-((R)-2,2-dimethyl-1,3-dioxolan-4-yl)-2,2-dimethyltetrahydrofuro[2,3-d] [1,3]dioxol-6-yl)-1H-1,2,3-triazol-4-yl) methoxy)-1-hydroxy-7-methoxy-9H-xanthen-9-one (17h)

Obtained as a yellow solid after flash chromatography purification (Hex-AcOEt 7:3) in 51 % yield. **^{1}H-NMR** (400 MHz, $CDCl_3$) δ: 12.82 (s, 1H), 7.81 (s, 1H), 7.55 (d, J = 2.8 Hz, 1H), 7.33 (d, J = 9.2 Hz, 1H), 7.28 (dd, J = 9.2 and 2.8 Hz, 1H), 6.48 (d, J = 2.0 Hz, 1H), 6.36 (d, J = 2.0 Hz, 1H), 6.25 (d, J = 3.6 Hz, 1H), 5.29 (s, 2H), 5.20 (d, J = 3.6 Hz, 1H), 5.01 (d, J = 3.6 Hz, 1H), 4.32 (dd, J = 9.2 and 3.6 Hz, 1H), 3.93–3.90 (comp, 2H), 3.88 (s, 3H), 3.08 (dt, J = 9.2 and 5.2 Hz, 1H), 1.58 (s, 3H), 1.42 (s, 3H), 1.37 (s, 3H), 1.16 (s, 3H); **^{13}C-NMR** (100 MHz, $CDCl_3$) δ: 180.7, 165.0, 163.4, 157.8, 156.2, 150.9, 142.8, 125.2, 125.0, 120.9, 119.1, 112.7, 109.8, 106.4, 105.3, 104.1, 97.8, 93.1, 83.5, 80.6, 72.3, 67.6, 66.0, 62.3, 56.0, 27.0, 26.8, 26.2, 25.0; **MS** (EI+) *m/z*: $[M]^+$; 581; **HRMS** *m/z* calcd for $^{12}C^{1}_{29}H^{14}_{31}N^{16}_{3}O_{10}$ $[M]^+$, 581.2009; found 581.2005; **IR** (ATR, cm^{-1}): 3146, 3085, 2988, 2937, 2917, 2897, 1655, 1608, 1574, 1484, 1278, 1216, 1199, 1165, 1149, 1077, 1033, 1012, 817, 778.

4.5.9. 9-((1-((3aR,5S,6S,6aR)-5-((R)-2,2-dimethyl-1,3-dioxolan-4-yl)-2,2-dimethyltetrahydrofuro[2,3-d] [1,3]dioxol-6-yl)-1H-1,2,3-triazol-4-yl) methoxy)-11-hydroxy-12H-benzo[a]xanthen-12-one (17i)

Obtained as a yellow solid after flash chromatography purification (Hex-AcOEt 7:3) in 42 % yield. **^{1}H-NMR** (400 MHz, $CDCl_3$) δ: 13.38 (s, 1H), 9.85 (d, J = 8.8 Hz, 1H), 8.03 (d, J = 9.2 Hz, 1H), 7.83 (s, 1H), 7.82 (d, J = 8.0 Hz, 1H), 7.71 (ddd, J = 8.4, 7.2, and 1.2 Hz, 1H), 7.54 (ddd, J = 8.0, 7.2, and 0.8 Hz, 1H), 7.40 (d, J = 9.2 Hz, 1H), 6.49 (d, J = 2.0 Hz, 1H), 6.37 (d, J = 2.0 Hz, 1H), 6.26 (d, J = 3.2 Hz, 1H), 5.27 (s, 2H), 5.21 (d, J = 3.6 Hz, 1H), 5.03 (d, J = 3.6 Hz, 1H), 4.34 (dd, J = 9.6 and 3.6 Hz, 1H), 3.94–3.92 (comp, 2H), 3.11 (dt, J = 9.2 and 5.6 Hz, 1H), 1.58 (s, 3H), 1.44 (s, 3H), 1.37 (s, 3H), 1.18 (s, 3H); **^{13}C-NMR** (100 MHz, $CDCl_3$) δ: 182.9, 164.3, 163.4, 157.6, 156.4, 142.8, 137.1, 130.7, 130.2, 129.6, 128.6, 126.8, 126.3, 125.2, 117.6, 113.2, 112.7, 109.9, 106.4, 105.6, 98.4, 92.6, 83.5, 80.6, 72.4, 67.7, 66.0, 62.3, 27.0, 26.8, 26.3, 25.0; **MS** (DART+) *m/z*: $[M+H]^+$; 602; **HRMS** *m/z* calcd for $^{12}C^{1}_{32}H^{14}_{32}N^{16}_{3}O_9$ $[M+H]^+$, 602.21385; found 602.21376; **IR** (ATR, cm^{-1}): 3124, 3090, 2982, 2932, 2900, 1659, 1581, 1511, 1451, 1209, 1174, 1160, 1077, 1048, 1027, 836, 825, 749.

4.5.10. (2R,3R,4S,5R,6R)-2-(acetoxymethyl)-6-(4-(((1-hydroxy-9-oxo-9H-xanthen-3-yl)oxy)methyl)-1H-1,2,3-triazol-1-yl)tetrahydro-2H-pyran-3,4,5-triyl triacetate (18a)

Obtained as a yellowish solid after flash chromatography purification (Hex-AcOEt 1:1) in 81 % yield. **^{1}H-NMR** (400 MHz, $CDCl_3$) δ: 12.83 (s, 1H), 8.21 (dd, J = 8.0 and 1.6 Hz, 1H), 7.92 (s, 1H), 7.69 (ddd, J = 8.4, 7.2, and 1.6 Hz, 1H), 7.41 (dd, J = 8.4 and 0.8 Hz, 1H), 7.35 (ddd, J = 8.0, 7.2, and 0.8 Hz, 1H), 6.51 (d, J = 2.4 Hz, 1H), 6.39 (d, J = 2.4 Hz, 1H), 5.92–5.90 (comp, 1H), 5.45–5.42 (comp, 2H), 5.27 (s, 2H), 5.27–5.22 (comp, 1H), 4.30 (dd, J = 12.8 and 4.8 Hz, 1H), 4.15 (dd, J = 12.8 and 2.0 Hz, 1H), 4.02 (ddd, J = 10.0, 4.8, and 2.0 Hz, 1H), 2.064 (s, 3H), 2.057 (s, 3H), 2.01 (s, 3H), 1.85 (s, 3H); **^{13}C-NMR** (100 MHz, $CDCl_3$) δ: 180.9, 170.6, 170.0, 169.4, 169.0, 165.1, 163.6, 157.8, 156.1, 143.9, 135.2, 125.9, 124.2, 121.6, 120.7, 117.7, 104.4, 97.8, 93.6, 85.9, 75.3, 72.6, 70.4, 67.8, 62.3, 61.6, 20.7, 20.61, 20.57, 20.2; **MS** (DART+)

m/z: $[M+H]^+$; 640; **HRMS** *m/z* calcd for $^{12}C^{1}_{30}H^{14}_{30}N^{16}_{3}O_{13}$ $[M+H]^+$, 640.17786; found 640.17742; **IR** (ATR, cm^{-1}): 3091, 2964, 2946, 2923, 2851, 1753, 1734, 1665, 1604, 1574, 1500, 1474, 1441, 1245, 1222, 1172, 1098, 1083, 1061, 1040, 766.

4.5.11. (2R,3R,4S,5R,6R)-2-(acetoxymethyl)-6-(4-(((1-hydroxy-6-methyl-9-oxo-9H-xanthen-3-yl)oxy)methyl)-1H-1,2,3-triazol-1-yl) tetrahydro-2H-pyran-3,4,5-triyl triacetate (18b)

Obtained as a yellowish solid after flash chromatography purification (Hex-AcOEt 1:1) in 51 % yield. **^{1}H-NMR** (400 MHz, $CDCl_3$) δ: 12.90 (s, 1H), 8.09 (d, J = 8.0 Hz, 1H), 7.92 (s, 1H), 7.204–7.199 (comp, 1H), 7.18–7.15 (comp, 1H), 6.49 (d, J = 2.4 Hz, 1H), 6.38 (d, J = 2.4 Hz, 1H), 5.92–5.89 (comp, 1H), 5.45–5.42 (comp, 2H), 5.27 (s, 2H), 5.27–5.22 (comp, 1H), 4.31 (dd, J = 12.4 and 4.8 Hz, 1H), 4.15 (dd, J = 12.4 and 2.0 Hz, 1H), 4.02 (ddd, J = 10.0, 4.8, and 2.0 Hz, 1H), 2.49 (s, 3H), 2.07 (s, 3H), 2.06 (s, 3H), 2.02 (s, 3H), 1.85 (s, 3H); **^{13}C-NMR** (100 MHz, $CDCl_3$) δ: 180.8, 170.6, 170.0, 169.4, 169.0, 164.9, 163.6, 157.8, 156.2, 146.9, 144.0, 125.70, 125.68, 121.5, 118.4, 117.5, 104.3, 97.7, 93.5, 85.9, 75.3, 72.7, 70.4, 67.8, 62.2, 61.6, 22.1, 20.8, 20.61, 20.58, 20.2; **MS** (DART+) *m/z*: $[M+H]^+$; 654; **HRMS** *m/z* calcd for $^{12}C^{1}_{31}H^{14}_{32}N^{16}_{3}O_{13}$ $[M+H]^+$, 654.19351; found 654.19353; **IR** (ATR, cm^{-1}): 3093, 2925, 2855, 1743, 1651, 1603, 1565, 1455, 1437, 1211, 1167, 1084, 1034, 817, 791.

4.5.12. (2R,3R,4S,5R,6R)-2-(acetoxymethyl)-6-(4-(((1-hydroxy-6-methoxy-9-oxo-9H-xanthen-3-yl)oxy)methyl)-1H-1,2,3-triazol-1-yl) tetrahydro-2H-pyran-3,4,5-triyl triacetate (18c)

Obtained as a yellowish solid after flash chromatography purification (Hex-AcOEt 1:1) in 49 % yield. **^{1}H-NMR** (400 MHz, $CDCl_3$) δ: 12.96 (s, 1H), 8.12 (d, J = 8.8 Hz, 1H), 7.91 (s, 1H), 6.92 (dd, J = 8.8 and 2.4 Hz, 1H), 6.81 (d, J = 2.4 Hz, 1H), 6.48 (d, J = 2.0 Hz, 1H), 6.38 (d, J = 2.0 Hz, 1H), 5.92–5.89 (comp, 1H), 5.45–5.42 (comp, 2H), 5.27 (s, 2H), 5.27–5.22 (comp, 1H), 4.31 (dd, J = 12.8 and 4.8 Hz, 1H), 4.15 (dd, J = 12.8 and 2.0 Hz, 1H), 4.02 (ddd, J = 10.2, 4.8, and 2.0 Hz, 1H), 3.92 (s, 3H), 2.07 (s, 3H), 2.06 (s, 3H), 2.02 (s, 3H), 1.85 (s, 3H); **^{13}C-NMR** (100 MHz, $CDCl_3$) δ: 180.2, 170.6, 170.0, 169.4, 169.0, 165.5, 164.6, 163.6, 158.1, 157.8, 144.0, 127.4, 121.5, 114.4, 113.4, 104.0, 100.2, 97.8, 93.5, 85.9, 75.3, 72.7, 70.4, 67.8, 62.2, 61.6, 56.0, 20.8, 20.61, 20.58, 20.2; **MS** (DART+) *m/z*: $[M+H]^+$; 670; **HRMS** *m/z* calcd for $^{12}C^{1}_{31}H^{14}_{32}N^{16}_{3}O_{14}$ $[M+H]^+$, 670.18843; found 670.18846; **IR** (ATR, cm^{-1}): 3091, 2925, 2848, 1739, 1651, 1600, 1568, 1499, 1446, 1240, 1212, 1167, 1085, 1032, 820, 796.

4.5.13. (2R,3R,4S,5R,6R)-2-(acetoxymethyl)-6-(4-(((1-hydroxy-6-fluoro-9-oxo-9H-xanthen-3-yl)oxy)methyl)-1H-1,2,3-triazol-1-yl) tetrahydro-2H-pyran-3,4,5-triyl triacetate (18d)

Obtained as a white solid after flash chromatography purification (Hex-AcOEt 1:1) in 50 % yield. **^{1}H-NMR** (400 MHz, $CDCl_3$) δ: 12.69 (s, 1H), 8.23–8.19 (comp, 1H), 7.93 (s, 1H), 7.09–7.05 (comp, 2H), 6.49 (d, J = 2.4 Hz, 1H), 6.39 (d, J = 2.4 Hz, 1H), 5.92–5.90 (comp, 1H), 5.45–5.42 (comp, 2H), 5.26 (s, 2H), 5.26–5.22 (comp, 1H), 4.30 (dd, J = 12.6 and 5.0 Hz, 1H), 4.15 (dd, J = 12.6 and 2.0 Hz, 1H), 4.02 (ddd, J = 10.2, 5.0, and 2.0 Hz, 1H), 2.06 (s, 3H), 2.05 (s, 3H), 2.01 (s, 3H), 1.85 (s, 3H); **^{13}C-NMR** (100 MHz, $CDCl_3$) δ: 179.9, 170.6, 170.0, 169.4, 169.0, 166.7 (d, J = 255.0 Hz), 165.1, 163.7, 157.8, 157.3 (d, J = 14.0 Hz), 143.8, 128.5 (d, J = 11.0 Hz), 121.6, 117.5 (d, J = 3.0 Hz), 112.9 (d, J = 22.0 Hz), 104.5 (d, J = 25.0 Hz), 104.0, 98.1, 93.8, 85.9, 75.3, 72.6, 70.4, 67.8, 62.3, 61.6, 20.7, 20.60, 20.57, 20.2; **MS** (DART+) *m/z*: $[M+H]^+$; 658; **HRMS** *m/z* calcd for $^{12}C^{1}_{30}H^{19}_{29}F^{14}_{1}N^{16}_{3}O_{13}$ $[M+H]^+$, 658.16844; found 658.16875; **IR** (ATR, cm^{-1}): 3077, 2921, 2850, 1756, 1742, 1661, 1608, 1586, 1498, 1448, 1246, 1224, 1210, 1166, 1150, 1101, 1067, 1039, 1023, 792.

4.5.14. (2R,3R,4S,5R,6R)-2-(acetoxymethyl)-6-(4-(((5,7-dichloro-1-hydroxy-9-oxo-9H-xanthen-3-yl)oxy)methyl)-1H-1,2,3-triazol-1-yl) tetrahydro-2H-pyran-3,4,5-triyl triacetate (18e)

Obtained as a yellow solid after flash chromatography purification (Hex-AcOEt 65:35) in 13 % yield. **^{1}H-NMR** (400 MHz, $CDCl_3$) δ: 12.44 (s, 1H), 8.11 (d, J = 2.8 Hz, 1H), 7.91 (s, 1H), 7.75 (d, J = 2.8 Hz, 1H), 6.64 (d, J = 2.4 Hz, 1H), 6.46 (d, J = 2.4 Hz, 1H), 5.91–5.89 (comp, 1H), 5.44–5.41 (comp, 2H), 5.31 (s, 2H), 5.27–5.22 (comp, 1H), 4.32 (dd, J = 12.8 and 5.2 Hz, 1H), 4.16 (dd, J = 12.8 and 2.0 Hz, 1H), 4.02 (ddd, J = 10.0, 5.2, and 2.0 Hz, 1H), 2.08 (s, 3H), 2.07 (s, 3H), 2.02 (s, 3H), 1.87 (s, 3H); **^{13}C-NMR** (100 MHz, $CDCl_3$) δ: 179.1, 170.6, 170.0, 169.4, 169.0, 165.7, 163.6, 157.2, 150.4, 143.7, 135.0, 129.6, 124.1, 123.8, 122.6, 121.5, 104.0, 98.7, 94.2, 86.0, 75.4, 72.6, 70.4, 67.7, 62.5, 61.6, 20.8, 20.61, 20.58, 20.2; **MS** (DART+) *m/z*: $[M+H]^+$; 708; **HRMS** *m/z* calcd for $^{12}C^{1}_{30}H^{35}_{28}Cl^{14}_{2}N^{16}_{3}O_{13}$ $[M+H]^+$, 708.09992; found 708.09979; **IR** (ATR, cm^{-1}): 3075, 2926, 2853, 1746, 1651, 1625, 1595, 1562, 1467, 1263, 1217, 1196, 1150, 1085, 1064, 1038, 832, 814, 799, 723.

4.5.15. (2R,3R,4S,5R,6R)-2-(acetoxymethyl)-6-(4-(((1-hydroxy-12-oxo-12h-benzo[b]xanthen-3-yl)oxy)methyl)-1H-1,2,3-triazol-1-yl)tetrahydro-2H-pyran-3,4,5-triyl triacetate (18f)

Obtained as a yellow solid after flash chromatography purification (Hex-AcOEt 1:1) in 34 % yield. **^{1}H-NMR** (400 MHz, $CDCl_3$) δ: 12.91 (s, 1H), 8.82 (s, 1H), 8.03 (d, J = 8.0 Hz, 1H), 7.93 (s, 1H), 7.88 (d, J = 8.0 Hz, 1H), 7.80 (s, 1H), 7.61 (ddd, J = 8.0, 6.8, and 1.2 Hz, 1H), 7.50 (ddd, J = 8.0, 6.8, and 1.2 Hz, 1H), 6.53 (d, J = 2.4 Hz, 1H), 6.40 (d, J = 2.4 Hz, 1H), 5.92–5.90 (comp, 1H), 5.48–5.40 (comp, 2H), 5.31 (s, 2H), 5.28–5.23 (comp, 1H), 4.32 (dd, J = 12.8 and 4.8 Hz, 1H), 4.16 (dd, J = 12.8 and 2.0 Hz, 1H), 4.02 (ddd, J = 10.0, 4.8, and 2.0 Hz, 1H), 2.08 (s, 3H), 2.07 (s, 3H), 2.02 (s, 3H), 1.87 (s, 3H); **^{13}C-NMR** (100 MHz, $CDCl_3$) δ: 181.5, 170.6, 170.0, 169.4, 169.0, 165.6, 164.2, 158.2, 152.0, 143.9, 136.9, 129.8, 129.7, 129.4, 127.7, 127.2, 125.8, 121.5, 120.3, 113.3, 103.8, 97.4, 93.9, 86.0, 75.4, 72.6, 70.4, 67.8, 62.3, 61.6, 20.8, 20.61, 20.58, 20.2; **MS** (DART+) *m/z*: $[M+H]^+$; 690; **HRMS** *m/z* calcd for $^{12}C^{1}_{34}H^{14}_{32}N^{16}_{3}O_{13}$ $[M+H]^+$, 690.19351; found 690.19330; **IR** (ATR, cm^{-1}): 3083, 2927, 2855, 1746, 1644, 1614, 1600, 1569, 1469, 1450, 1247, 1217, 1174, 1101, 1086, 1030, 816.

4.5.16. (2R,3R,4S,5R,6R)-2-(acetoxymethyl)-6-(4-(((1-hydroxy-5-methoxy-9-oxo-9H-xanthen-3-yl)oxy)methyl)-1H-1,2,3-triazol-1-yl) tetrahydro-2H-pyran-3,4,5-triyl triacetate (18g)

Obtained as a yellow solid after flash chromatography purification (Hex-AcOEt 1:1) in 63 % yield. **^{1}H-NMR** (400 MHz, $CDCl_3$) δ: 12.79 (s, 1H), 7.92 (s, 1H), 7.77 (dd, J = 8.0 and 1.6 Hz, 1H), 7.26 (t, J = 8.0 Hz, 1H), 7.20 (dd, J = 8.0 and 1.6 Hz, 1H), 6.60 (d, J = 2.4 Hz, 1H), 6.39 (d, J = 2.4 Hz, 1H), 5.91 (d, J = 9.2 Hz, 1H), 5.48–5.39 (comp, 2H), 5.26 (s, 2H), 5.27–5.22 (comp, 1H), 4.30 (dd, J = 12.8 and 5.2 Hz, 1H), 4.15 (dd, J = 12.8 and 2.0 Hz, 1H), 4.02 (ddd, J = 10.0, 4.8, and 2.0 Hz, 1H), 3.99 (s, 3H), 2.06 (s, 3H), 2.05 (s, 3H), 2.01 (s, 3H), 1.85 (s, 3H); **^{13}C-NMR** (100 MHz, $CDCl_3$) δ: 180.9, 170.6, 170.0, 169.4, 169.0, 165.1, 163.4, 157.6, 148.4, 146.4, 143.9, 123.8, 121.5, 116.8, 115.8, 104.4, 98.3, 93.5, 85.9, 75.3, 72.7, 70.3, 67.7, 62.3, 61.6, 56.5, 20.7, 20.60, 20.57, 20.2; **MS** (DART+) *m/z*: $[M+H]^+$; 670; **HRMS** *m/z* calcd for $^{12}C^{1}_{31}H^{14}_{32}N^{16}_{3}O_{14}$ $[M+H]^+$, 670.18843; found 670.18861; **IR** (ATR, cm^{-1}): 3095, 2943, 2846, 1742, 1646, 1621, 1608, 1574, 1492, 1439, 1247, 1216, 1204, 1153, 1101, 1046, 1028, 729.

4.5.17. (2R,3R,4S,5R,6R)-2-(acetoxymethyl)-6-(4-(((1-hydroxy-7-methoxy-9-oxo-9H-xanthen-3-yl)oxy)methyl)-1H-1,2,3-triazol-1-yl) tetrahydro-2H-pyran-3,4,5-triyl triacetate (18h)

Obtained as a yellow solid after flash chromatography purification (Hex-AcOEt 1:1) in 57 % yield. **^{1}H-NMR** (400 MHz, $CDCl_3$) δ: 12.81 (s, 1H), 7.94 (s, 1H), 7.52 (d, J = 2.8 Hz, 1H), 7.31 (d, J = 9.2 Hz, 1H), 7.25 (dd, J = 9.2 and 2.8 Hz, 1H), 6.45 (d, J = 2.0 Hz, 1H), 6.35 (d, J = 2.0 Hz, 1H), 5.92 (d, J = 8.8 Hz, 1H), 5.46 (t, J = 8.8 Hz, 1H), 5.42 (t, J = 8.8 Hz, 1H), 5.28–5.22 (comp, 1H), 5.25 (s, 2H), 4.29 (dd, J = 12.4 and

5.2 Hz, 1H), 4.14 (dd, $J = 12.4$ and 2.0 Hz, 1H), 4.02 (ddd, $J = 10.0$, 5.2, and 2.0 Hz, 1H), 3.86 (s, 3H), 2.05 (s, 6H), 2.00 (s, 3H), 1.84 (s, 3H); **^{13}C-NMR** (100 MHz, $CDCl_3$) δ: 180.6, 170.6, 170.0, 169.4, 169.0, 164.9, 163.4, 157.7, 156.1, 150.8, 143.9, 125.0, 121.6, 120.8, 119.0, 105.2, 104.0, 97.7, 93.2, 85.9, 75.3, 72.7, 70.4, 67.8, 62.2, 61.6, 56.0, 20.7, 20.60, 20.57, 20.2; **MS** (EI+) *m/z*: $[M]^+$; 669; **HRMS** *m/z* calcd for $^{12}C^1_{31}H^{14}_{31}N^{16}_3O_{14}$ $[M]^+$, 669.1806; found 669.1793; **IR** (ATR, cm^{-1}): 3078, 2940, 2850, 1746, 1651, 1608, 1485, 1212, 1162, 1149, 1104, 1064, 1027, 813, 776.

4.5.18. (2R,3R,4S,5R,6R)-2-(acetoxymethyl)-6-(4-(((11-hydroxy-12-oxo-12h-benzo[a]xanthen-9-yl)oxy)methyl)-1H-1,2,3-triazol-1-yl) tetrahydro-2H-pyran-3,4,5-triyl triacetate (18i)

Obtained as a yellow solid after flash chromatography purification (Hex-AcOEt 1:1) in 42 % yield. **^{1}H-NMR** (400 MHz, $CDCl_3$) δ: 13.37 (s, 1H), 9.82 (d, $J = 8.8$ Hz, 1H), 8.01 (d, $J = 9.2$ Hz, 1H), 7.95 (s, 1H), 7.80 (d, $J = 8.0$ Hz, 1H), 7.68 (ddd, $J = 8.4$, 6.8, and 1.2 Hz, 1H), 7.52 (ddd, $J = 8.0$, 6.8, and 0.8 Hz, 1H), 7.38 (d, $J = 8.8$ Hz, 1H), 6.47 (d, $J = 2.0$ Hz, 1H), 6.37 (d, $J = 2.0$ Hz, 1H), 5.93 (d, $J = 8.8$ Hz, 1H), 5.48 (t, $J = 9.6$ Hz, 1H), 5.43 (t, $J = 9.6$ Hz, 1H), 5.27 (d, $J = 10.0$ Hz, 1H), 5.24 (s, 2H), 4.31 (dd, $J = 12.4$ and 4.8 Hz, 1H), 4.15 (dd, $J = 12.4$ and 2.0 Hz, 1H), 4.03 (ddd, $J = 10.0$, 4.8, and 2.0 Hz, 1H), 2.06 (s, 6H), 2.01 (s, 3H), 1.85 (s, 3H); **^{13}C-NMR** (100 MHz, $CDCl_3$) δ: 182.9, 170.6, 170.0, 169.5, 169.0, 164.2, 163.4, 157.6, 156.4, 144.0, 137.1, 130.7, 130.2, 129.6, 128.6, 126.7, 126.2, 121.6, 117.6, 113.1, 105.6, 98.3, 92.7, 85.9, 75.3, 72.7, 70.4, 67.8, 62.2, 61.6, 20.7, 20.62, 20.58, 20.2; **MS** (DART+) *m/z*: $[M+H]^+$; 690; **HRMS** *m/z* calcd for $^{12}C^1_{34}H^{14}_{32}N^{16}_3O_{13}$ $[M+H]^+$, 690.19351; found 690.19341; **IR** (ATR, cm^{-1}): 3079, 2941, 1743, 1652, 1585, 1514, 1450, 1248, 1212, 1158, 1090, 1060, 1030, 824.

4.6. α-Glucosidase inhibition

Inhibition was evaluated using a previously reported method [11]. A solution (25 μL) of tested samples in DMSO-H_2O (1:1) was added to 150 μL of phosphate buffer solution (PBS, 67 mM, pH 6.8) and incubated at 37 °C for 10 min with 25 μL of reduced glutathione (3 mM in PBS) and 25 μL of 0.1 U mL^{-1} in PBS solution of α-glucosidase type I (Sigma cat. G5003-100UN). The substrate solution (25 μL, 23.2 mM *p*-nitrophenyl-α-D-glucopyranoside, Sigma N1377-1G, in PBS) was added and incubated at 37 °C for 15 min with shaking. The reaction mixture was quenched with 50 μL of 1 M Na_2CO_3 solution, and after 5 min of agitation, the optical density was determined at 405 nm. Quercetin was used as the positive standard. The inhibition percentage was calculated with the equation:

$$\text{Inhibition (\%)} = [(\text{A control} - \text{A sample})/\text{A control}] \times 100$$

where A = the absorbance at 405 nm of the sample and control.

4.7. Lineweaver-Burk plots

To determine the kinetics of enzyme inhibitors, concentrations of 1/2 × IC_{50}, IC_{50}, and 2 × IC_{50} were selected. With each inhibitor's concentration, the α-glucosidase activity was assayed by varying *p*-nitrophenyl-α-D-glucopyranoside (pNPG) concentration from 1 to 23.1 mM. The kinetic inhibition was carried out similarly to the α-glucosidase inhibition protocol. The enzyme and inhibitor were preincubated for 10 min, and the reaction was carried out with different concentrations of pNPG at 37 °C. Immediately, the absorbance at 405 nm was measured (T0). Then, the absorbance was measured every 2 min for 10 min. The Lineweaver-Burk plots were constructed to assess the kinetics of enzyme inhibition.

4.8. In vivo studies

4.8.1. Experimental animals

Male CD-1 mice (*Mus musculus*) –weighing 30 ± 5 g at 6–8 weeks of age– were obtained from the Animal Handling Unit for Teaching and Research (UMADI) of the Metropolitan Autonomous University. Mice were fed with standard rodent food (Harlan Laboratories, Indianapolis, USA) and water *ad libitum* under a 12 h light/12 h dark cycle. The experimental protocol adhered to the International Rules for the Care and Use of Laboratory Animals, in agreement with the Mexican Official Norm (NOM-062-ZOO-1999, 2001 revision).

4.8.2. Streptozotocin (STZ)-induced diabetic model

Mice were induced to experimental diabetes by the administration of an initial intraperitoneal dose of 40 mg/kg of nicotinamide (NAM) and, 20 min later, a dose of 100 mg/kg of streptozotocin (STZ) dissolved in freshly prepared 0.1 M citrate buffer (pH 4.5). Subsequently, glycemia was measured to ensure that mice developed hyperglycemia. Mice with glycemic levels over 160 mg/dL were considered adequate for assays. Blood samples were collected from the caudal vein. The blood glucose concentration was estimated using a commercial glucometer (Accu-Chek Performa; Roche, Mannheim, Germany) [30].

4.8.3. Oral sucrose tolerance test (OSTT)

Normoglycemic mice were randomly divided into four groups (n = 5): control (saline solution), acarbose (50 mg/kg), compound **17f** (50 mg/kg), and compound **18f** (50 mg/kg). Mice were fasted for 12 h with free access to tap water throughout the experiment. Fasting glucose levels were considered as time 0. Control and test compounds were administered orally. Thirty minutes after administration of the test samples, a dose of 2 g/kg sucrose solution was administered. Then, glycemia was measured at 30, 60, 90, and 120 min after sucrose administration, employing a glucometer (Accu-Chek Performa; Roche, Mannheim, Germany). The same procedure was followed for diabetic mice, with a modification: diabetic animals were fasted for 8 h.

The percentage variation of glycemia for each group was calculated in relation to the initial (0 h) level, according to the formula:

$$\text{\% variation of glycemia} = [(Gx - G0)/G0] \times 100$$

where G0 was the initial glycemia value and Gx were the glycemia values at each time, respectively [30].

4.8.4. Statistical analysis

Data is shown as mean ± standard error of the mean (n = 5). One-way ANOVA followed by Dunnett's multiple comparisons test was performed using GraphPad Prism version 10.2.3 for Windows. Values of $p \leq 0.05$ (*), $p \leq 0.01$ (**), $p \leq 0.001$ (***), and $p \leq 0.0001$ (****) were considered statistically significant.

4.9. Artemia salina acute toxicity test

4.9.1. Hatching shrimp

Brine shrimp cysts, *Artemia salina*, were hatched in commercial artificial seawater (Instant Ocean, Aquarium Systems, Inc., USA), dissolving 38 g of sea salt in 1 L of distilled water. After an incubation period (48 h) in a conical container at room temperature (25 ± 2 °C), under light and continuous aeration with an aquarium pump, the nauplii (stage II and III) were attracted with light to one side of the container, collected with a Pasteur pipette, and transferred to a Petri dish. Afterward, 10 larvae were transferred to a 96-well microplate with 100 μL of artificial seawater.

4.9.2. Brine shrimp assay

The brine shrimp lethality test monitored the acute toxicity of the samples and the solvent. A stock solution was prepared in DMSO at a

concentration of 20 mg/mL. Aliquots of the samples were diluted in distilled water to obtain the desired final concentration. Assay was performed in 96-well microplates (Corning, NY, USA). Each well contained 10 larvae in 100 μL of seawater. 100 μL of each sample dilution were transferred to the wells; each concentration was tested in triplicate. Negative control wells contained 10 larvae in artificial seawater only (200 μL). Additionally, the effect of 5 % DMSO and distilled water (100 μL) was tested. Potassium dichromate (in distilled water) served as a positive control [47]. The microplate was incubated for 24 h, then examined in an inverted Nikon microscope, and the number of dead larvae in each well was counted and recorded after 24 h. The mortality endpoint was defined as the absence of forward motion of shrimps [48]. The percentage of larval mortality was determined after 24 h exposure to the different concentrations of the tested compounds, using the Reed-Muench method [47].

4.10. Sulforhodamine B assay

The biological assay was performed in accordance with previous work [49]. The cell line was cultured in RPMI-1640 medium supplemented with 10 % fetal bovine serum, 2 mM L-glutamine, 10,000 units per mL penicillin G sodium, 10 μgmL^{-1} streptomycin sulfate, 25 μgmL^{-1} amphotericin B (Gibco), and 1 % non-essential amino acids (Gibco). The cultures were maintained at 37 °C in a 5 % CO_2-humidified atmosphere. The viability of the cells used in the experiments exceeded 95 % (determined by trypan blue). The cells were removed from the tissue culture flasks by trypsin treatment and diluted with fresh medium. 100 μL cell suspension aliquots, containing 5000–10,000 cells per well, were transferred into 96-well microtiter plates (Costar) and incubated at 37 °C for 24 h in a 5 % CO_2 atmosphere. Stock solutions of the tested compounds initially dissolved in DMSO (20 mM) were prepared and further diluted in the medium to obtain the desired concentrations. One-hundred-microliter aliquots of xanthone solutions were added to each well (50 μM) and then incubated for 48 h. After that, cells were fixed to the plastic substratum by the addition of 50 μL of cold 50 % aqueous trichloroacetic acid. The plates were incubated at 4 °C for 1 h, washed with tap H_2O, and air-dried. The trichloroacetic acid-fixed cells were stained by the addition of 0.4 % Sulforhodamine B (SRB). The free SRB solution was removed by washing with 1 % aqueous acetic acid. The plates were air-dried, and the bound dye was solubilized by the addition of 100 μL of 10 mM unbuffered Tris base; then, they were placed on a shaker for 5 min before analysis. Optical densities were determined using an Ultra Microplated Reader (Elx 808, BIO-TEX Instruments, Inc.), $\lambda = 515$ nm.

4.11. Molecular docking

Ligands (**17a-i**, **18a-i**, and **4a**) were modeled and minimized with Avogadro (version 1.2.0) using the MMFF94 force field [50]. The α-glucosidase model was obtained from the AlphaFold Protein Structure Database using the Uniprot identification P3815811. Molecular docking was performed employing the Glide software from Schrödinger [43,44] (version 2024-3) in accordance with the established protocols provided by the software developers. The protein and ligands were prepared with the modules "Protein preparation" and "Ligprep", respectively. The grid box was centered at the allosteric site (coordinates: x = 14.15, y = 3.98, and z = 3.67), with a size of 20 × 20 × 20 Å, using the Receptor grid generation tool. Ligands were docked into the allosteric site using the extra precision (XP) algorithm. Binding poses, interactions, and edition of figures were obtained from the same docking suite.

4.12. Molecular dynamics simulations

All molecular dynamics simulations were performed using AMBER22 with the FF19SB force field for proteins and the pmemd.cuda module [51–53]. Compound **17f** was parameterized using the Antechamber module within AMBER, employing the General AMBER Force Field for organic molecules [54]. Atomic partial charges were assigned using the AM1-BCC method [55].

The protonation states of titratable residues were assigned to reflect a physiological pH value of 6.8, using PDBFixer and PropKa3 [56,57]. Accordingly, Glu276, Glu296, Glu376, Asp440, Asp214, His251, His279, and His97 were modeled in their protonated forms. The enzyme–ligand complex was solvated in a truncated octahedral box with explicit OPC water molecules [58], extending 11 Å beyond any solute atom in all directions. The system charge was neutralized by adding the appropriate number of Na^+ counterions.

Energy minimization was first performed to remove steric clashes and optimize solvent orientation, using a combination of 2000 steps of steepest descent followed by 3000 steps of conjugate gradient minimization. During this stage, Cartesian restraints (4.0 kcal mol^{-1} $Å^{-2}$) were applied to the heavy atoms of the protein. The system was then subjected to a multi-stage equilibration protocol. The temperature gradually increased from 100 K to 300 K in four consecutive NVT heating stages of 200 ps each, corresponding to target temperatures of 150, 200, 250, and 300 K. Langevin dynamics was used for temperature control, with a collision frequency of 4 ps^{-1} for the first three stages and 2 ps^{-1} for the final stage. Harmonic restraints were applied to all heavy atoms of the protein, with decreasing force constants of 5.0, 4.0, 3.0, and 1.0 kcal mol^{-1} $Å^{-2}$, allowing gradual relaxation of the structure.

Following heating, the system was equilibrated for 1 ns in the NPT ensemble at 300 K and 1 bar, employing the Monte Carlo barostat [59] (pressure relaxation time of 2 ps) and maintaining the same 1.0 kcal mol^{-1} $Å^{-2}$ positional restraints. Periodic boundary conditions were applied, and long-range electrostatic interactions were treated using particle mesh Ewald [60] with a real-space cutoff of 10 Å. The same cutoff was used for Lennard–Jones interactions. All bonds involving hydrogen atoms were constrained using the SHAKE algorithm [61]. The hydrogen mass repartitioning scheme [62] was applied using ParmEd [56], allowing an integration time step of 4 fs. Production MD simulations were performed in the NPT ensemble at 310 K and 1 bar, using the same thermostat and barostat conditions as NPT equilibration. Each trajectory was 100 ns in length, and five independent replicas were generated for the enzyme-ligand complex.

To identify representative ligand conformations sampled during the simulations, k-means clustering [63] was applied using the cpptraj module of AmberTools22 [64]. All heavy atoms of the xanthone **17f** were included in the analysis. Before clustering, the trajectories were aligned to the protein backbone to remove overall rotational and translational motions. The k-means algorithm partitions the conformational space into a predefined number of clusters, minimizing the total within-cluster variance by iteratively assigning structures to the nearest centroid and updating the centroid positions. A total of four clusters were used.

Molecular visualizations were generated using UCSF ChimeraX v1.9 [65,66].

CRediT authorship contribution statement

Carlos D. García-Mejía: Writing – original draft, Methodology, Investigation. **Julio César Almanza-Pérez:** Resources, Methodology, Investigation. **Luis Fernando Cofas-Vargas:** Validation, Methodology. **Abigail Aragón-Morales:** Methodology. **Antonio Nieto-Camacho:** Investigation, Conceptualization. **Enrique García-Hernández:** Writing – review & editing, Validation, Supervision, Software. **Eduardo Hernández-Vázquez:** Writing – original draft, Validation, Supervision, Software, Resources, Project administration, Methodology, Investigation, Funding acquisition, Formal analysis, Data curation, Conceptualization.

Declaration of competing interest

The authors declare that they have no known competing financial interests or personal relationships that could have appeared to influence the work reported in this paper.

Acknowledgments

Financial support from PAPIIT, UNAM (IN213625) is gratefully acknowledged. Carlos D. García-Mejía thanks the SECIHTI for the postgraduate studies scholarship. The authors are grateful for the analytical support from the "Instituto de Química, UNAM", especially to M. C. Elizabeth Huerta-Salazar (NMR support). Moreover, the authors thank M. C. Maria Teresa Ramírez-Apán for the cytotoxicity studies and Dr. Fernanda Artemisa Espinoza-Hernández for statistical analysis counseling. We would like to thank to Animal Management Unit for Teaching and Research (UMADI) at Universidad Autónoma Metropolitana-Iztapalapa, Mexico, for technical support. Luis Fernando Cofas-Vargas acknowledges Polish high-performance computing infrastructure PLGrid (HPC Center: ACK Cyfronet AGH) for providing computer facilities and support within computational grants no. PLG/2024/017332 and PLG/2025/018510.

Appendix A. Supplementary data

Supplementary data to this article can be found online at https://doi.org/10.1016/j.ejmech.2025.118384.

Data availability

Data will be made available on request.

References

[1] R.A. DeFronzo, E. Ferrannini, L. Groop, R.R. Henry, W.H. Herman, J.J. Holst, F. B. Hu, C.R. Kahn, I. Raz, G.I. Shulman, D.C. Simonson, M.A. Testa, R. Weiss, Type 2 diabetes mellitus, Nat. Rev. Dis. Primers 1 (1) (2015) 15019, https://doi.org/10.1038/nrdp.2015.19.

[2] Y. Zheng, S.H. Ley, F.B. Hu, Global aetiology and epidemiology of type 2 diabetes mellitus and its complications, Nat. Rev. Endocrinol. 14 (2) (2018) 88–98, https://doi.org/10.1038/nrendo.2017.151.

[3] D. Magliano, E.J. Boyko, IDF Diabetes Atlas, tenth ed., International Diabetes Federation, Brussels, 2021.

[4] J.J. Marín-Peñalver, I. Martín-Timón, C. Sevillano-Collantes, F.J.D. Cañizo-Gómez, Update on the treatment of type 2 diabetes mellitus, World J. Diabetes 7 (17) (2016) 354–395, https://doi.org/10.4239/wjd.v7.i17.354.

[5] A. Barmak, K. Niknam, G. Mohebbi, Synthesis, structural studies, and α-Glucosidase inhibitory, antidiabetic, and antioxidant activities of 2,3-Dihydroquinazolin-4(1*H*)-Ones derived from Pyrazol-4-Carbaldehyde and anilines, ACS Omega 4 (19) (2019) 18087–18099, https://doi.org/10.1021/acsomega.9b01906.

[6] J.-L. Chiasson, R.G. Josse, J.A. Hunt, C. Palmason, N.W. Rodger, S.A. Ross, E. A. Ryan, M.H. Tan, T.M.S. Wolever, The efficacy of acarbose in the treatment of patients with Non–insulin-dependent diabetes mellitus: a multicenter, controlled clinical trial, Ann. Intern. Med. 121 (12) (1994) 928–935, https://doi.org/10.7326/0003-4819-121-12-199412150-00004.

[7] P. Segal, P.U. Feig, G. Schernthaner, K.P. Ratzmann, J. Rybka, D. Petzinna, C. Berlin, The efficacy and safety of miglitol therapy compared with glibenclamide in patients with NIDDM inadequately controlled by diet alone, Diabetes Care 20 (5) (1997) 687–691, https://doi.org/10.2337/diacare.20.5.687.

[8] J.-L. Chiasson, R.G. Josse, R. Gomis, M. Hanefeld, A. Karasik, M. Laakso, for The STOP-NIDDM Trial Research Group, Acarbose treatment and the risk of cardiovascular disease and hypertension in patients with impaired glucose tolerance: the STOP-NIDDM trial, JAMA 290 (4) (2003) 486–494, https://doi.org/10.1001/jama.290.4.486.

[9] D.S.H. Bell, Type 2 diabetes mellitus: what is the optimal treatment regimen? Am. J. Med. 116 (5) (2004) 23–29, https://doi.org/10.1016/j.amjmed.2003.10.017.

[10] A.M. Dirir, M. Daou, A.F. Yousef, L.F. Yousef, A review of alpha-glucosidase inhibitors from plants as potential candidates for the treatment of Type-2 diabetes, Phytochem. Rev. 21 (4) (2022) 1049–1079, https://doi.org/10.1007/s11101-021-09773-1.

[11] E. Hernández-Vázquez, S. Martínez-Caballero, D. Aldana-Torres, S. Estrada-Soto, A. Nieto-Camacho, Discovery of dual-action phenolic 4-Arylidene-Isoquinolinones with antioxidant and α-Glucosidase inhibition activities, RSC Med. Chem. 15 (2) (2024) 519–538, https://doi.org/10.1039/D3MD00585B.

[12] Shagufta, I. Ahmad, Recent insight into the biological activities of synthetic xanthone derivatives, Eur. J. Med. Chem. 116 (2016) 267–280, https://doi.org/10.1016/j.ejmech.2016.03.058.

[13] D.I.S.P. Resende, F. Durães, M. Maia, E. Sousa, M.M.M. Pinto, Recent advances in the synthesis of xanthones and azaxanthones, Org. Chem. Front. 7 (19) (2020) 3027–3066, https://doi.org/10.1039/D0QO00659A.

[14] Y. Liu, L. Zou, L. Ma, W.-H. Chen, B. Wang, Z.-L. Xu, Synthesis and pharmacological activities of xanthone derivatives as α-Glucosidase inhibitors, Bioorg. Med. Chem. 14 (16) (2006) 5683–5690, https://doi.org/10.1016/j.bmc.2006.04.014.

[15] Y. Liu, L. Ma, W.-H. Chen, B. Wang, Z.-L. Xu, Synthesis of xanthone derivatives with extended π-Systems as α-Glucosidase inhibitors: insight into the probable binding mode, Bioorg. Med. Chem. 15 (8) (2007) 2810–2814, https://doi.org/10.1016/j.bmc.2007.02.030.

[16] G.-J. Ye, T. Lan, Z.-X. Huang, X.-N. Cheng, C.-Y. Cai, S.-M. Ding, M.-L. Xie, B. Wang, Design and synthesis of novel xanthone-triazole derivatives as potential antidiabetic agents: α-glucosidase inhibition and glucose uptake promotion, Eur. J. Med. Chem. 177 (2019) 362–373, https://doi.org/10.1016/j.ejmech.2019.05.045.

[17] G.-L. Li, C.-Y. Cai, J.-Y. He, L. Rao, L. Ma, Y. Liu, B. Wang, Synthesis of 3-Acyloxyxanthone derivatives as α-Glucosidase inhibitors: a further insight into the 3-Substituents' effect, Bioorg. Med. Chem. 24 (7) (2016) 1431–1438, https://doi.org/10.1016/j.bmc.2016.01.022.

[18] A. Nagy, B. Csordás, V. Zsoldos-Mády, I. Pintér, V. Farkas, A. Perczel, C-3 epimers of sugar amino acids as foldameric building blocks: improved synthesis, useful derivatives, coupling strategies, Amino Acids 49 (2) (2017) 223–240, https://doi.org/10.1007/s00726-016-2346-5.

[19] I.L. Deras, K. Takegawa, A. Kondo, I. Kato, Y.C. Lee, Synthesis of a high-mannose-type glycopeptide analog containing a glucose-asparagine linkage, Bioorg. Med. Chem. Lett. 8 (13) (1998) 1763–1766, https://doi.org/10.1016/S0960-894X(98)00306-0.

[20] T. Zhou, Q. Shi, C.-H. Chen, L. Huang, P. Ho, S.L. Morris-Natschke, K.-H. Lee, Anti-AIDS agents 85. Design, synthesis, and evaluation of 1R,2R-Dicamphanoyl-3,3-Dimethyldihydropyrano-[2,3-c]Xanthen-7(1*H*)-One (DCX) derivatives as novel Anti-HIV agents, Eur. J. Med. Chem. 47 (2012) 86–96, https://doi.org/10.1016/j.ejmech.2011.10.025.

[21] S. Moreau, M. Varache-Lembège, S. Larrouture, D. Fall, A. Neveu, G. Deffieux, J. Vercauteren, A. Nuhrich, (2-Arylhydrazonomethyl)-Substituted xanthones as antimycotics: synthesis and fungistatic activity against *candida* species, Eur. J. Med. Chem. 37 (3) (2002) 237–253, https://doi.org/10.1016/S0223-5234(01)01332-0.

[22] D.A. Garcia Cortez, M.C.M. Young, A. Marston, J.-L. Wolfender, K. Xanthones Hostettmann, Triterpenes and a biphenyl from *Kielmeyera coriacea*, Phytochemistry 47 (7) (1998) 1367–1374, https://doi.org/10.1016/S0031-9422(97)00731-0.

[23] A.C. Muñoz-Estrada, C.E. Tovar-Roman, C.D. García-Mejía, R. García-Contreras, E. Hernández-Vázquez, Diversity-oriented synthesis and antibiofilm evaluation of Furan-2-Carboxamides, ChemMedChem 20 (9) (2025) e202400879, https://doi.org/10.1002/cmdc.202400879.

[24] C.W. Choi, Y.H. Choi, M.-R. Cha, D.S. Yoo, Y.S. Kim, G.H. Yon, K.S. Hong, Y. H. Kim, S.Y. Ryu, Yeast α-Glucosidase inhibition by isoflavones from plants of leguminosae as an in vitro alternative to acarbose, J. Agric. Food Chem. 58 (18) (2010) 9988–9993, https://doi.org/10.1021/jf101926j.

[25] Á. Ramírez-Trinidad, E. Martínez-Solano, C.E. Tovar-Roman, M. García-Guerrero, J.A. Rivera-Chávez, E. Hernández-Vázquez, Synthesis, antibiofilm activity and molecular docking of N-Acylhomoserine lactones containing cinammic moieties, Bioorg. Med. Chem. Lett. 98 (2024) 129592, https://doi.org/10.1016/j.bmcl.2023.129592.

[26] M.-J. Kim, S.-B. Lee, H.-S. Lee, S.-Y. Lee, J.-S. Baek, D. Kim, T.-W. Moon, J.F. Robyt, K.-H. Park, Comparative study of the inhibition of α-Glucosidase, α-Amylase, and cyclomaltodextrin glucanosyltransferase by acarbose, isoacarbose, and Acarviosine–Glucose, Arch. Biochem. Biophys. 371 (2) (1999) 277–283, https://doi.org/10.1006/abbi.1999.1423.

[27] A.A. Tahrani, M.K. Piya, A. Kennedy, A.H. Barnett, Glycaemic control in type 2 diabetes: targets and new therapies, Pharmacol. Ther. 125 (2) (2010) 328–361, https://doi.org/10.1016/j.pharmthera.2009.11.001.

[28] G. Libralato, E. Prato, L. Migliore, A.M. Cicero, L. Manfra, A review of toxicity testing protocols and endpoints with *Artemia* spp, Ecol. Indic. 69 (2016) 35–49, https://doi.org/10.1016/j.ecolind.2016.04.017.

[29] X. Araya, M. Okumu, G. Durán, A. Gómez, J.M. Gutiérrez, G. León, Assessment of the *Artemia salina* toxicity assay as a substitute of the mouse lethality assay in the determination of venom-induced toxicity and preclinical efficacy of antivenom, Toxicon X 22 (2024) 100195, https://doi.org/10.1016/j.toxcx.2024.100195.

[30] W. Rosiles-Alanis, A. Zamilpa, R. García-Macedo, M.A. Zavala-Sánchez, S. Hidalgo-Figueroa, B. Mora-Ramiro, R. Román-Ramos, S.E. Estrada-Soto, J.C. Almanza-Perez, 4-Hydroxybenzoic acid and β -Sitosterol from *Cucurbita ficifolia* act as insulin secretagogues, peroxisome proliferator-activated receptor-gamma agonists, and liver glycogen storage promoters: *in vivo* , *in vitro* , and *in silico* studies, J. Med. Food 25 (6) (2022) 588–596, https://doi.org/10.1089/jmf.2021.0071.

[31] C.O. Eleazu, K.C. Eleazu, S. Chukwuma, U.N. Essien, Review of the mechanism of cell death resulting from streptozotocin challenge in experimental animals, its practical use and potential risk to humans, J. Diabetes Metab. Disord. 12 (1) (2013) 60, https://doi.org/10.1186/2251-6581-12-60.

[32] S.M. Lee, S.A. Bustamante, O. Koldovský, The effect of alpha-glucosidase inhibition on intestinal disaccharidase activity in normal and diabetic mice, Metabolism 32 (8) (1983) 793–799, https://doi.org/10.1016/0026-0495(83)90109-9.

[33] W.F. Caspary, A.M. Rhein, W. Creutzfeldt, Increase of intestinal brush border hydrolases in mucosa of streptozotocin-diabetic rats, Diabetologia 8 (6) (1972) 412–414, https://doi.org/10.1007/BF01212169.
[34] L. Liu, Y.-L. Yu, C. Liu, X.-T. Wang, X.-D. Liu, L. Xie, Insulin deficiency induces abnormal increase in intestinal disaccharidase activities and expression under diabetic states, evidences from in vivo and in vitro study, Biochem. Pharmacol. 82 (12) (2011) 1963–1970, https://doi.org/10.1016/j.bcp.2011.09.014.
[35] Y. Li, P. Zhao, Y. Chen, Y. Fu, K. Shi, L. Liu, H. Liu, M. Xiong, Q.-H. Liu, G. Yang, Y. Xiao, Depsidone and xanthones from *Garcinia xanthochymus* with hypoglycemic activity and the mechanism of promoting glucose uptake in L6 myotubes, Bioorg. Med. Chem. 25 (24) (2017) 6605–6613, https://doi.org/10.1016/j.bmc.2017.10.043.
[36] S.-P. Chen, S.-R. Lin, T.-H. Chen, H.-S. Ng, H.-S. Yim, M.K. Leong, C.-F. Weng, Mangosteen xanthone γ-Mangostin exerts lowering blood glucose effect with potentiating insulin sensitivity through the mediation of AMPK/PPARγ, Biomed. Pharmacother. 144 (2021) 112333 https://doi.org/10.1016/j.biopha.2021.112333.
[37] F. Zhong, Y. Chen, G. Yang, Chemical constituents from the bark of *Garcinia xanthochymus* and their 1,1-Diphenyl-2-picrylhydrazyl (DPPH) radical-scavenging activities, Helv. Chim. Acta 91 (9) (2008) 1695–1703, https://doi.org/10.1002/hlca.200890185.
[38] C.M.M. Santos, M. Freitas, D. Ribeiro, A. Gomes, A.M.S. Silva, J.A.S. Cavaleiro, E. Fernandes, 2,3-Diarylxanthones as strong scavengers of reactive oxygen and nitrogen species: a structure–activity relationship study, Bioorg. Med. Chem. 18 (18) (2010) 6776–6784, https://doi.org/10.1016/j.bmc.2010.07.044.
[39] Z.X. Lu, M. Hasmeda, W. Mahabusarakam, B. Ternai, P.C. Ternai, G.M. Polya, Inhibition of eukaryote protein kinases and of a cyclic nucleotide-binding phosphatase by prenylated xanthones, Chem. Biol. Interact. 114 (1–2) (1998) 121–140, https://doi.org/10.1016/S0009-2797(98)00049-0.
[40] L. Saraiva, P. Fresco, E. Pinto, E. Sousa, M. Pinto, J. Gonçalves, Inhibition of protein kinase C by synthetic xanthone derivatives, Bioorg. Med. Chem. 11 (7) (2003) 1215–1225, https://doi.org/10.1016/S0968-0896(02)00641-7.
[41] C.N. Nguyen, B.T.D. Trinh, T.B. Tran, L.-T.T. Nguyen, A.K. Jäger, L.-H.D. Nguyen, Anti-diabetic xanthones from the bark of *Garcinia xanthochymus*, Bioorg. Med. Chem. Lett. 27 (15) (2017) 3301–3304, https://doi.org/10.1016/j.bmcl.2017.06.021.
[42] Z.P. Li, Y.H. Song, Z. Uddin, Y. Wang, K.H. Park, Inhibition of protein tyrosine phosphatase 1B (PTP1B) and α-Glucosidase by xanthones from *Cratoxylum cochinchinense*, and their kinetic characterization, Bioorg. Med. Chem. 26 (3) (2018) 737–746, https://doi.org/10.1016/j.bmc.2017.12.043.
[43] R.A. Friesner, J.L. Banks, R.B. Murphy, T.A. Halgren, J.J. Klicic, D.T. Mainz, M. P. Repasky, E.H. Knoll, M. Shelley, J.K. Perry, D.E. Shaw, P. Francis, P.S. Shenkin, Glide: a new approach for rapid, accurate docking and scoring. 1. Method and assessment of docking accuracy, J. Med. Chem. 47 (7) (2004) 1739–1749, https://doi.org/10.1021/jm0306430.
[44] R.A. Friesner, R.B. Murphy, M.P. Repasky, L.L. Frye, J.R. Greenwood, T.A. Halgren, P.C. Sanschagrin, D.T. Mainz, Extra precision glide: docking and scoring incorporating a model of hydrophobic enclosure for protein−ligand complexes, J. Med. Chem. 49 (21) (2006) 6177–6196, https://doi.org/10.1021/jm051256o.
[45] K. Liu, H. Kokubo, Exploring the stability of ligand binding modes to proteins by molecular dynamics simulations: a cross-docking study, J. Chem. Inf. Model. 57 (10) (2017) 2514–2522, https://doi.org/10.1021/acs.jcim.7b00412.
[46] L.P. Avila-Barrientos, L.F. Cofas-Vargas, G. Agüero-Chapin, E. Hernández-García, S. Ruiz-Carmona, N.A. Valdez-Cruz, M. Trujillo-Roldán, J. Weber, Y.B. Ruiz-Blanco, X. Barril, E. García-Hernández, Computational design of inhibitors targeting the catalytic β subunit of *Escherichia coli* FOF1-ATP synthase, Antibiotics 11 (5) (2022) 557, https://doi.org/10.3390/antibiotics11050557.
[47] S.M. Colegate, R.J. Molyneux, Bioactive Natural Products: Detection, Isolation, and Structural Determination, second ed., CRC Press, 2007.
[48] M. Favilla, L. Macchia, A. Gallo, C. Altomare, Toxicity assessment of metabolites of fungal biocontrol agents using two different (*Artemia salina* and *Daphnia magna*) invertebrate bioassays, Food Chem. Toxicol. 44 (11) (2006) 1922–1931, https://doi.org/10.1016/j.fct.2006.06.024.
[49] C.D. García-Mejía, E. Hernández-Vázquez, J. Alejandro Ibarra-Hernández, A. Tarbuck-Valle, M.T. Ramírez-Apán, A regioselective synthesis of 3,4-Diaryl-1*H*-Pyrazoles through a 1,3-Dipolar cycloaddition of tosylhydrazones and nitroalkenes, Org. Biomol. Chem. 21 (30) (2023) 6205–6217, https://doi.org/10.1039/D3OB00753G.
[50] M.D. Hanwell, D.E. Curtis, D.C. Lonie, T. Vandermeersch, E. Zurek, G. R. Avogadro Hutchison, An advanced semantic chemical editor, visualization, and analysis platform, J. Cheminf. 4 (1) (2012) 17, https://doi.org/10.1186/1758-2946-4-17.
[51] D.A. Case, H.M. Aktulga, K. Belfon, I.Y. Ben-Shalom, J.T. Berryman, S.R. Brozell, D. S. Cerutti, T.E. Cheatham III, G.A. Cisneros, V.W.D. Cruzeiro, T.A. Darden, R. E. Duke, G. Giambasu, M.K. Gilson, H. Gohlke, A.W. Goetz, R. Harris, S. Izadi, S. A. Izmailov, K. Kasavajhala, M.C. Kaymak, E. King, A. Kovalenko, T. Kurtzman, T. S. Lee, S. LeGrand, P. Li, C. Lin, J. Liu, T. Luchko, R. Luo, M. Machado, V. Man, M. Manathunga, K.M. Merz, Y. Miao, O. Mikhailovskii, G. Monard, H. Nguyen, K. A. O'Hearn, A. Onufriev, F. Pan, S. Pantano, R. Qi, A. Rahnamoun, D.R. Roe, A. Roitberg, C. Sagui, S. Schott-Verdugo, A. Shajan, J. Shen, C.L. Simmerling, N. R. Skrynnikov, J. Smith, J. Swails, R.C. Walker, J. Wang, J. Wang, H. Wei, R. M. Wolf, X. Wu, Y. Xiong, Y. Xue, D.M. York, S. Zhao, P.A. Kollman, Amber 2022, University of California, San Francisco, 2022, https://doi.org/10.13140/RG.2.2.31337.77924.
[52] R. Salomon-Ferrer, D.A. Case, R.C. Walker, An overview of the amber biomolecular simulation package, WIREs Comput. Mol. Sci. 3 (2) (2013) 198–210, https://doi.org/10.1002/wcms.1121.
[53] C. Tian, K. Kasavajhala, K.A.A. Belfon, L. Raguette, H. Huang, A.N. Migues, J. Bickel, Y. Wang, J. Pincay, Q. Wu, C. Simmerling, ff19SB: amino-acid-specific protein backbone parameters trained against quantum mechanics energy surfaces in solution, J. Chem. Theor. Comput. 16 (1) (2020) 528–552, https://doi.org/10.1021/acs.jctc.9b00591.
[54] X. He, V.H. Man, W. Yang, T.-S. Lee, J. Wang, A fast and high-quality charge model for the next generation general AMBER force field, J. Chem. Phys. 153 (11) (2020) 114502, https://doi.org/10.1063/5.0019056.
[55] A. Jakalian, D.B. Jack, C.I. Bayly, Fast, efficient generation of high-quality atomic charges. AM1-BCC model: II. Parameterization and validation, J. Comput. Chem. 23 (16) (2002) 1623–1641, https://doi.org/10.1002/jcc.10128.
[56] P. Eastman, J. Swails, J.D. Chodera, R.T. McGibbon, Y. Zhao, K.A. Beauchamp, L.-P. Wang, A.C. Simmonett, M.P. Harrigan, C.D. Stern, R.P. Wiewiora, B.R. Brooks, V.S. Pande, OpenMM 7: rapid development of high performance algorithms for molecular dynamics, PLoS Comput. Biol. 13 (7) (2017) e1005659, https://doi.org/10.1371/journal.pcbi.1005659.
[57] M.H.M. Olsson, C.R. Søndergaard, M. Rostkowski, J.H. Jensen, PROPKA3: consistent treatment of internal and surface residues in empirical p K_a predictions, J. Chem. Theor. Comput. 7 (2) (2011) 525–537, https://doi.org/10.1021/ct100578z.
[58] S. Izadi, R. Anandakrishnan, A.V. Onufriev, Building water models: a different approach, J. Phys. Chem. Lett. 5 (21) (2014) 3863–3871, https://doi.org/10.1021/jz501780a.
[59] J. Åqvist, P. Wennerström, M. Nervall, S. Bjelic, B.O. Brandsdal, Molecular dynamics simulations of water and biomolecules with a monte carlo constant pressure algorithm, Chem. Phys. Lett. 384 (4–6) (2004) 288–294, https://doi.org/10.1016/j.cplett.2003.12.039.
[60] T. Darden, D. York, L. Pedersen, Particle mesh ewald: an $N \cdot \log(N)$ method for ewald sums in large systems, J. Chem. Phys. 98 (12) (1993) 10089–10092, https://doi.org/10.1063/1.464397.
[61] J.-P. Ryckaert, G. Ciccotti, H.J.C. Berendsen, Numerical integration of the Cartesian equations of motion of a system with constraints: molecular dynamics of *n*-Alkanes, J. Comput. Phys. 23 (3) (1977) 327–341, https://doi.org/10.1016/0021-9991(77)90098-5.
[62] C.W. Hopkins, S. Le Grand, R.C. Walker, A.E. Roitberg, Long-time-step molecular dynamics through hydrogen mass repartitioning, J. Chem. Theor. Comput. 11 (4) (2015) 1864–1874, https://doi.org/10.1021/ct5010406.
[63] J.A. Hartigan, M.A. Wong, Algorithm AS 136: a K-Means clustering algorithm, Appl. Stat. 28 (1) (1979) 100, https://doi.org/10.2307/2346830.
[64] D.R. Roe, T.E. Cheatham, PTRAJ and CPPTRAJ: software for processing and analysis of molecular dynamics trajectory data, J. Chem. Theor. Comput. 9 (7) (2013) 3084–3095, https://doi.org/10.1021/ct400341p.
[65] E.C. Meng, T.D. Goddard, E.F. Pettersen, G.S. Couch, Z.J. Pearson, J.H. Morris, T. E. Ferrin, UCSF ChimeraX : tools for structure building and analysis, Protein Sci. 32 (11) (2023) e4792, https://doi.org/10.1002/pro.4792.
[66] E.F. Pettersen, T.D. Goddard, C.C. Huang, E.C. Meng, G.S. Couch, T.I. Croll, J. H. Morris, T.E. Ferrin, UCSF ChimeraX : structure visualization for researchers, educators, and developers, Protein Sci. 30 (1) (2021) 70–82, https://doi.org/10.1002/pro.3943.